Research Paper

The ZiBuPiYin recipe regulates proteomic alterations in brain mitochondria-associated ER membranes caused by chronic psychological stress exposure: implications for cognitive decline in Zucker diabetic fatty rats

Huiying Xu[1], Wen Zhou[1], Libin Zhan[1], Hua Sui[2], Lijing Zhang[1], Chunyan Zhao[1], Xiaoguang Lu[3]

[1]Modern Research Laboratory of Spleen Visceral Manifestations Theory, School of Traditional Chinese Medicine and School of Integrated Chinese and Western Medicine, Nanjing University of Chinese Medicine, Nanjing 210023, China
[2]Institute of Integrative Medicine, Dalian Medical University, Dalian 116044, China
[3]Department of Emergency Medicine, Zhongshan Hospital, Dalian University, Dalian 116001, China

Correspondence to: Libin Zhan, Xiaoguang Lu; **email:** zlbnj@njucm.edu.cn, luxiaoguang@dlu.edu.cn
Keywords: psychological stress, diabetes-associated cognitive decline, mitochondria-associated ER membrane, proteomics, ZiBuPiYin recipe
Received: January 21, 2020 **Accepted:** July 23, 2020 **Published:** November 18, 2020

ABSTRACT

Chronic psychological stress (PS) cumulatively affects memory performance through the deleterious effects on hypothalamic-pituitary-adrenal axis regulation. Several functions damaged in cognitive impairment-related diseases are regulated by mitochondria-associated ER membranes (MAMs). To elucidate the role of ZiBuPiYin recipe (ZBPYR) in regulating the MAM proteome to improve PS-induced diabetes-associated cognitive decline (PSD), differentially expressed MAM proteins were identified among Zucker diabetic fatty rats, PSD rats, and PS combined with ZBPYR administration rats via iTRAQ with LC-MS/MS. Proteomic analysis revealed that the expressions of 85 and 33 proteins were altered by PS and ZBPYR treatment, respectively. Among these, 21 proteins were differentially expressed under both PS and ZBPYR treatments, whose functional categories included energy metabolism, lipid and protein metabolism, and synaptic dysfunction. Furthermore, calcium signaling and autophagy-related proteins may play roles in the pathogenesis of PSD and the mechanism of ZBPYR, respectively. Notably, KEGG pathway analysis suggested that 'Alzheimer's disease' and 'oxidative phosphorylation' pathways may be impaired in PSD pathogenesis, while ZBPYR could play a neuroprotective role through regulating the above pathways. Overall, exposure to chronic PS contributes to the evolution of diabetes-associated cognitive decline and ZBPYR might prevent and treat PSD by regulating the MAM proteome.

INTRODUCTION

Stress is a necessary, adaptive mechanism for survival in its acute form; however, prolonged stress is considered to be a key issue that impacts health by causing the over-activation of stress-activated systems. Chronic activation of the hypothalamic-pituitary-adrenal (HPA) axis may occur following chronic psychological stress (PS), accompanied by a continuous increase in adreno-corticotropic hormone (ACTH) and glucocorticoid (GC; primarily corticosterone in rodents) concentrations.

Studies have shown that psychological stress is considered as one of the important risk factors of T2DM [1]. From a biological perspective, chronic PS primarily induces insulin resistance by affecting the emotional loop of the hypothalamus and limbic systems. Diabetes-associated cognitive decline (DACD) is generally

considered to be a central nervous system (CNS) complication of diabetes, and its pathogenesis primarily includes HPA axis dysregulation, brain insulin resistance, oxidative stress, mitochondrial damage, inflammatory response, and calcium homeostasis imbalance [2, 3]. However, the impact of PS, particularly long-term PS exposure, on DACD has not been thoroughly investigated.

Under a state of chronic PS, the sustained activation of the HPA axis can lead to the simultaneous occurrence of mitochondrial dysfunction and endoplasmic reticulum (ER) stress. Mitochondria and the ER are interrelated both in physiology and function and this link can be attributed to the physical interaction between the two organelles through the mitochondria-associated ER membrane (MAM). MAM is enriched with dozens of proteins and plays an important role in a variety of processes including mitochondrial dynamics and homeostasis, lipid metabolism, calcium homeostasis, and autophagy [4]. Continuing proteomics studies have demonstrated MAM protein changes in mice and humans, as well as in T2DM and cognitive dysfunction [5, 6]. Since MAM functions as a hub for both neurodegeneration [4] and metabolic disease [7], comprehensive knowledge of the protein composition of MAM will be extremely useful in elucidating the mechanisms of PS-induced diabetes-associated cognitive decline (PSD).

The ZiBuPiYin recipe (ZBPYR) is a modification of the Zicheng Decoction, which was recorded in the book of Bujuji written by Cheng Wu in the Qing dynasty, and has been used for the clinical treatment of cognitive impairment. Previous studies from our research group have demonstrated that ZBPYR improves learning and memory in rodents with dementia and DACD, and is related to the regulation of brain insulin resistance, Aβ production and degradation, dendritic spine density, and gut microbiota [8]. Therefore, it was deemed important to explore the molecular mechanisms linking the MAM proteome to PSD and ZBPYR treatment using isobaric tags for relative and absolute quantitation (iTRAQ) with liquid chemistry-mass spectrometry/mass spectrometry (LC-MS/MS) technology.

RESULTS

ZBPYR improves glucose metabolism in PSD rats

Random blood glucose (RBG) levels were not significantly different between ZDF, PSD, and PS combined with ZBPYR administration (PDZ) groups at week seven. Starting at week eight, the levels of RBG were continuously elevated in ZDF and PSD rats, while in the PDZ group they were significantly lower than those in the two other groups (Figure 1A). Within the oral glucose tolerance test (OGTT) and the insulin tolerance test (ITT), there were significant differences in fasting blood glucose levels between the PSD and PDZ groups (p <0.001), and the blood glucose in the PDZ group almost returned to the level of 0min at the final time point (Figure 1B–1E). It can be inferred, then, that the administration of ZBPYR obviously reduced blood glucose levels and enhanced insulin sensitivity.

ZBPYR regulates the activation of the HPA axis in PSD rats

In weeks 8 to 13, the concentration of ACTH in the PSD group was always significantly higher than that in the ZDF group (p <0.01, Figure 2A, 2B). Additionally, the corticosterone (CORT) concentration of the PSD group was significantly higher than that of the ZDF group at week 13 (p <0.0001, Figure 2C). Compared with the PSD group, the ACTH concentration in the PDZ group was significantly downregulated at weeks 8, 11, 12, 13, while the CORT concentration was significantly downregulated at week 13 (p <0.01, Figure 2A, 2C). Indeed, the administration of ZBPRY significantly attenuated the excessive sustained activation of the HPA axis.

ZBPYR regulates exploratory behaviors, spatial learning, and memory performance

In the open field test (OFT), the PSD rats entered the center less frequently compared with ZDF rats (p <0.05, Figure 3B). ZBPYR treatment significantly increased the number of entries into the center zone and vertical numbers (p <0.05, Figure 3B, 3D).

We used the Morris Water Maze (MWM) to measure the effects of different treatments on spatial learning and memory. In the hidden platform test, the escape latency of the ZDF group was shorter than that of the PSD group on days 3-5, while the PSD group escape latency was longer than the PDZ group on days 4 and 5 (p <0.01, Figure 3E). In the probe test, compared with the PSD group, the percentage of time spent in the correct quadrant and the platform crossing number were both significantly increased in the PDZ group (p <0.05, Figure 3F, 3G). Additionally, PDZ rats swam shorter distances and required less time to locate the original platform position (p <0.01, Figure 3H, 3I). In the visible platform version of the test, the escape latency of the PDZ group was shorter than that of the PSD group (p <0.05, Figure 3J). Indeed, ZBPYR administration evidently improved spontaneous locomotor activities and cognitive decline in the PSD group.

Validation of the purity of MAM fractions

To validate the quality of MAM preparations from rat brains, three independent methods were used. First, the

different steps of MAM preparation from ZDF rat brains (n=3) were quality controlled by western blot analysis (Figure 4A, 4B). The distribution trend of seven molecules, such as the MAM marker acyl-CoA synthetase long chain 4 (ACSL4/FACL4), in different fractions was consistent with previously published data [9, 10]. Secondly, LC-MS/MS protein identification of MAM preparations revealed that MAM fractions contained five known characteristic MAM proteins, namely Apoe, Fis1, S100B, Cisd2, and Bcap31 (Supplementary Table 1). Furthermore, 32 of these proteins are associated with cognitive impairment and 12 are associated with diabetes mellitus. Finally, according to the enrichment analysis of MAM samples, most of the enriched cellular components (e.g., mitochondrion and the ER), biological processes (e.g., cell redox homeostasis and glucose metabolic processes), molecular functions (e.g., GTP binding,

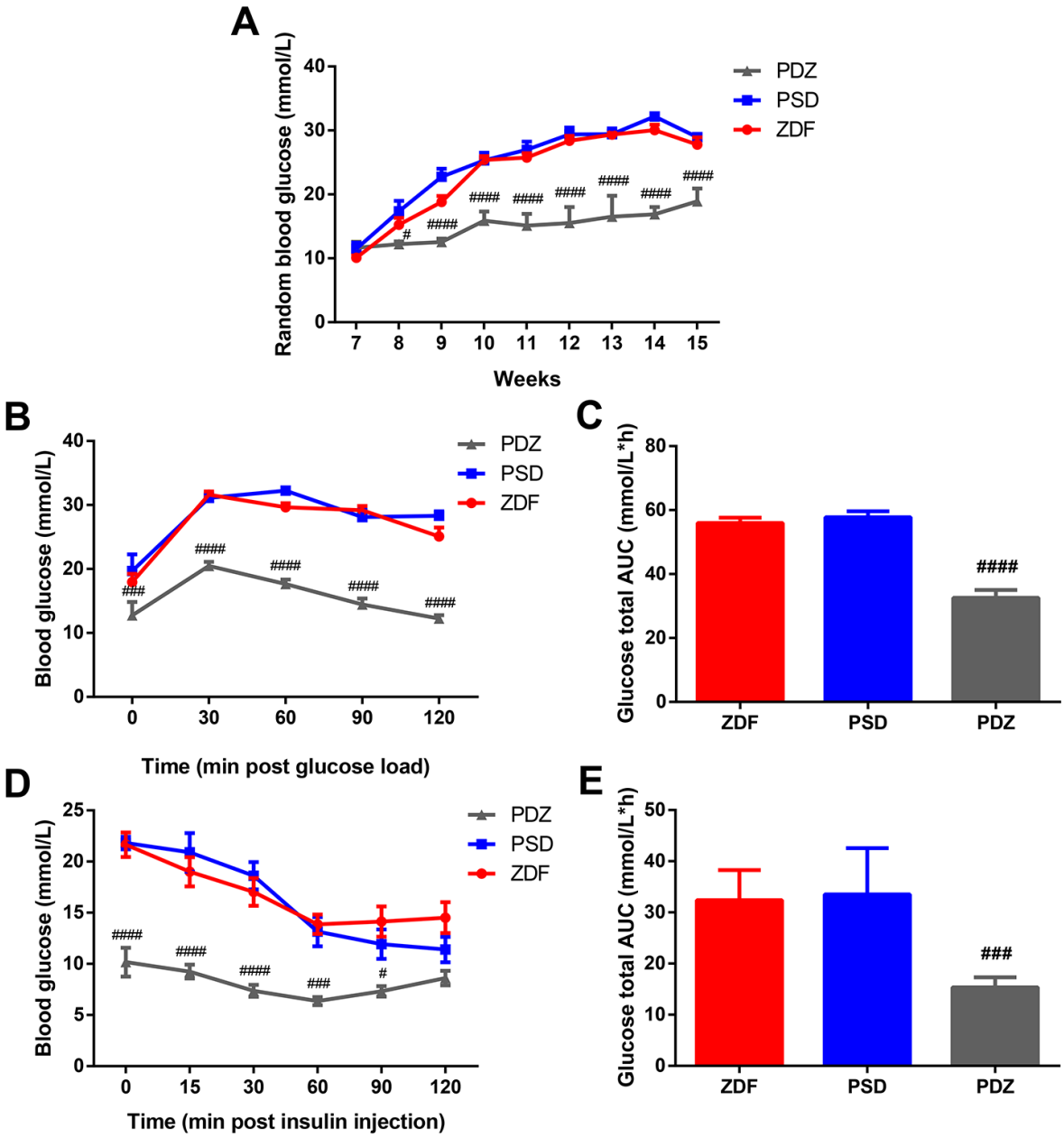

Figure 1. Effects of ZBPYR on RBG, glucose tolerance, and insulin resistance in PSD rats. (**A**) RBG was measured at 7-15 weeks old. Oral glucose tolerance tests were performed on 14 hour fasted rats after 10 weeks with a Purina 5008 diet. Blood glucose levels (**B**), total glucose area under the curve (AUC) (**C**). Insulin tolerance tests were conducted on 6 hour fasted animals. Blood glucose levels (**D**), total glucose AUC (**E**). $^{\#}p$ <0.05, $^{\#\#\#}p$ <0.001, $^{\#\#\#\#}p$ <0.0001 PDZ vs. PSD. ZDF: ZDF rats; PSD: ZDF rats treated with PS; PDZ: ZDF rats treated with PS combined with ZBPYR administration (mean ± SEM, n=6-8 per group).

NAD binding, and GTPase activity), and Kyoto Encyclopedia of Genes and Genomes (KEGG) pathways (e.g., Alzheimer's disease and oxidative phosphorylation) are strongly related to mitochondrial-ER processes (Figure 4C–4F).

Differentially-expressed brain MAM proteins between PSD:ZDF and PDZ:PSD groups

The entire proteomics workflow is shown in Figure 5. A total of 1,819 proteins were identified and 938 common proteins were successfully quantified from all individual samples. Both Venn diagram and Volcano plots both showed that chronic PS and ZBPYR treatment caused differential expressions of 85 and 33 proteins in brain MAMs, respectively. Furthermore, twenty-one overlapped proteins were differentially expressed in both PSD:ZDF and PDZ:PSD groups (Figure 6A–6C). Among the 85 proteins differentially expressed in the PSD:ZDF group, 36 of those were increased and 49 decreased (Figure 6D, Supplementary Table 2). The significantly increased MAM proteins included Bcap31, Lamp2, Krt10, Marcks, and Cct5, while those significantly decreased included Alg2, Gnb4, Cndp2, Vti1b, and ND2. Moreover, among the 33 proteins differentially expressed in PDZ:PSD group, 25 of those were increased and eight decreased (Figure 6E, Supplementary Table 3). The significantly increased MAM proteins included Alg2, Cndp2, Abhd12, Slc4a10, and S100b, while those significantly decreased included Nsfl1c, OMG, Mapk1, Mobp, and Eef1a2. Additionally, there were 21 overlapped proteins, namely Acot7, Abhd12, Apoe, Fdxr, Atp5, ND2, Pkm, Gapdh, Alg2, Rab5c, OMG, Mapk1, Gng12, Dbnl, Cndp2, Bcat1, Fis1, Txnrd2, Dnajb11, S100b, and Mag (Figure 6F, Supplementary Table 4).

Bioinformatics analysis of differentially expressed brain MAM proteins

Deep analyses based on the differentially expressed proteins (DEPs) including a gene ontology (GO) enrichment analysis, PPI network analysis, and KEGG pathway analysis, were also conducted.

In PSD:ZDF rats, altered biological processes included the strong enrichment of protein stabilization, response to sodium arsenite, and positive regulation of telomere

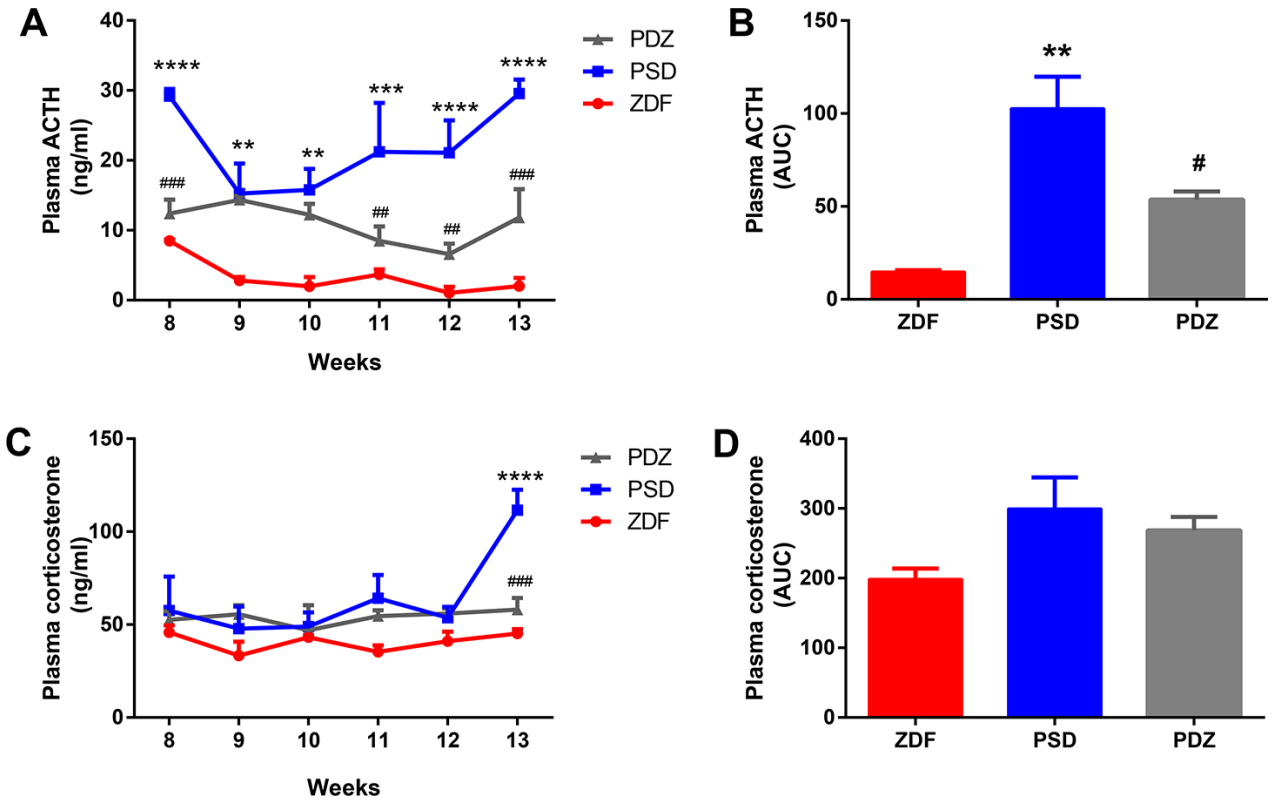

Figure 2. Effects of ZBPYR on plasma adrenocorticotropic hormone (ACTH) and corticosterone (CORT) during the stress intervention period in PSD rats. Plasma ACTH values were examined weekly. Plasma ACTH (**A**), ACTH AUC (**B**). Plasma corticosterone values were measured weekly. Plasma corticosterone (**C**), corticosterone AUC (**D**). $^{**}p$ <0.01, $^{***}p$ <0.001, $^{****}p$ <0.0001 PSD vs. ZDF; $^{\#}p$ <0.05, $^{\#\#}p$ <0.01, $^{\#\#\#}p$ <0.001 PDZ vs. PSD (mean ± SEM, n=3 per group).

maintenance via telomerase (Figure 7A). Cellular component annotation demonstrated a strong enrichment of the myelin sheath, extracellular exosome, and mitochondrion (Figure 7C). An analysis based on the molecular functions showed that the majority of the DEPs were associated with two major functions. One of these functions is binding, including protein binding, GTP binding, NAD binding, and identical protein binding. The other function is catalyst activity, including GTPase activity (Figure 7E). In the PDZ:PSD group, the biological process revealed that the DEPs primarily involved in cholesterol homeostasis, including cholesterol metabolic processes, regulation of cholesterol transport, and positive regulation of cholesterol efflux (Figure 7B). Additionally, a GO analysis showed similar results with those in the PSD:ZDF group in regards to cellular components and molecular functions (Figures 7D, 7F).

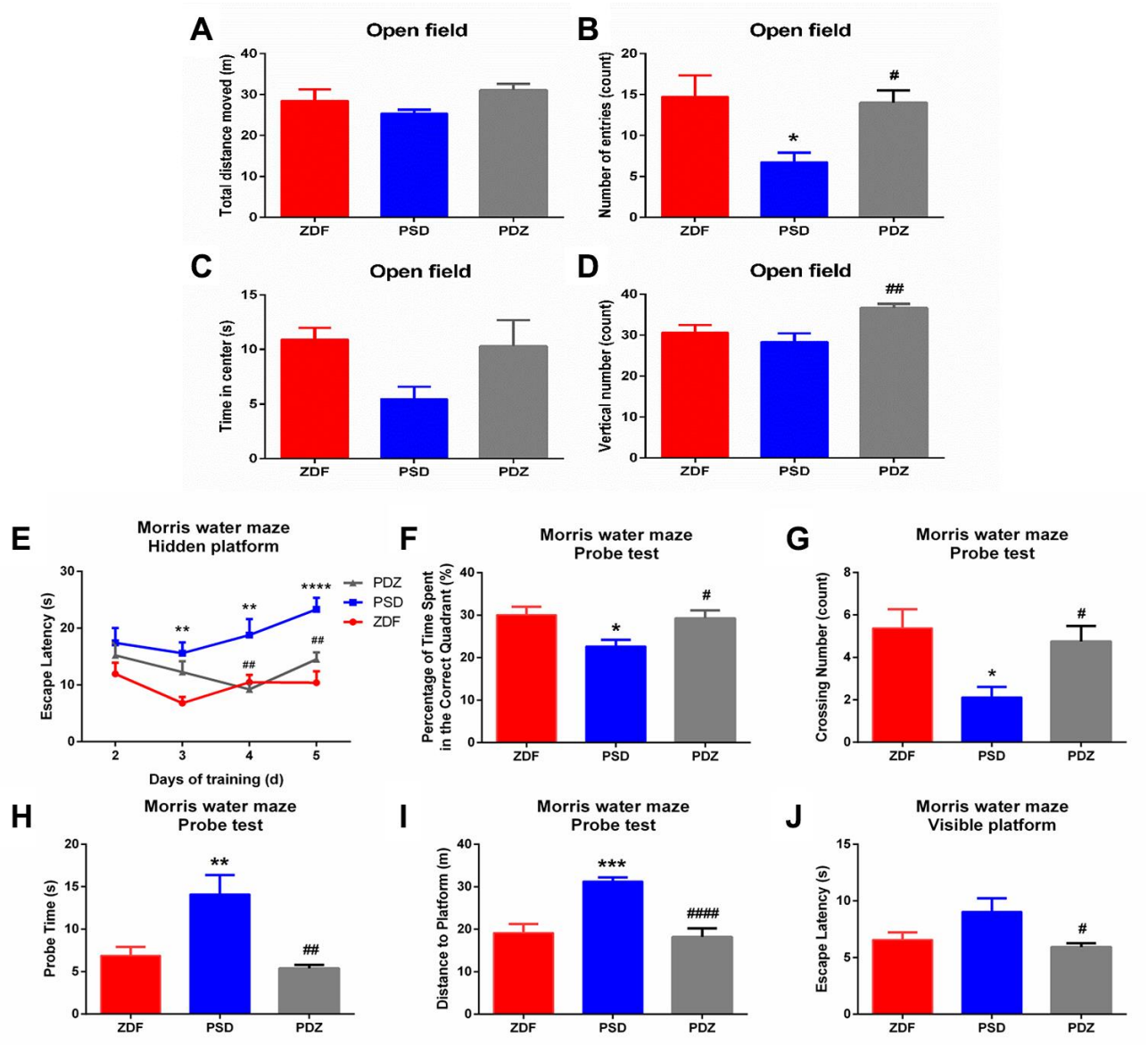

Figure 3. Effects of ZBPYR on behavioral performance of treatment in PSD rats. The OFT was performed during day 1 and the MWM was performed during days 2-7 of the last seven days. Spontaneous locomotor activities were recorded in the OFT, including total distance moved (**A**), number of center zone entries (**B**), time spent in the center (**C**), and vertical number (**D**). (**E**) Escape latencies were analyzed in the training trials of the MWM. Performance in the probe test was analyzed, including the percentage of time spent in the target quadrant (**F**), crossing number of the original platform location (**G**), probe time searching for the original platform location (**H**), and the distance traveled to the original platform location (**I**). (**J**) Escape latency in the visible platform version of the MWM was analyzed. $^{*}p$ <0.05, $^{**}p$ <0.01, $^{***}p$ <0.001, $^{****}p$ <0.0001 PSD vs. ZDF; $^{\#}p$ <0.05, $^{\#\#}p$ <0.01, $^{\#\#\#\#}p$ <0.0001, PDZ vs. PSD (mean ± SEM, n=8 per group).

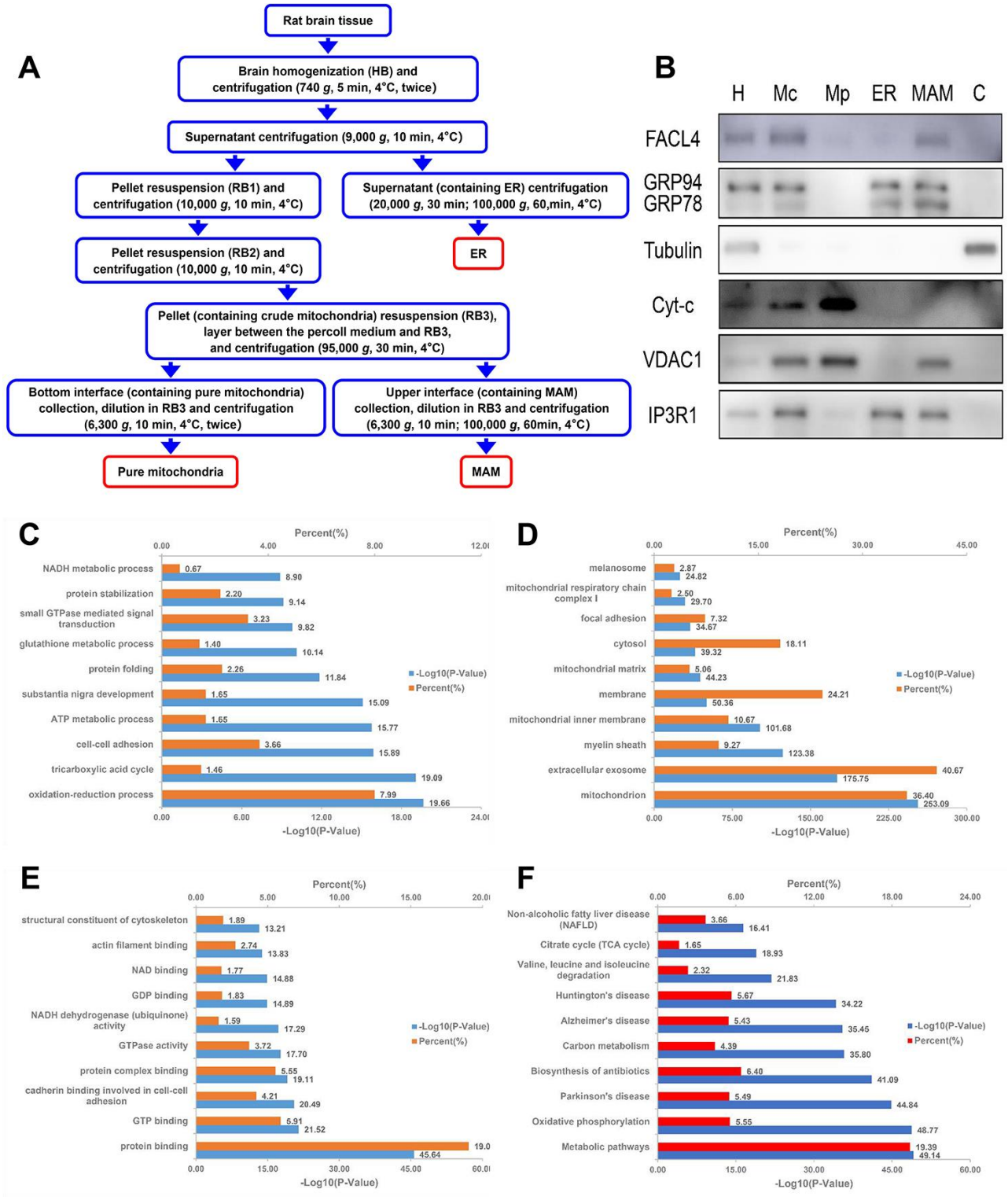

Figure 4. Schematic diagram of MAM isolation and purity confirmation of the MAM fraction by WB and enrichment analysis. (**A**) MAM was isolated from ZDF rat brains by applying differential centrifugation and self-forming Percoll gradient centrifugation. Other cell organelles, such as crude mitochondria, pure mitochondria, and ER were similarly obtained following the multiple centrifuge steps. (**B**) Western blot analysis of organelle markers in isolated MAM from the brain were enriched for FACL4 and KDEL, and were free from tubulin and cytochrome-C contamination. H: homogenate; Mp: pure mitochondria; Mc: crude mitochondria; ER: endoplasmic reticulum; MAM: mitochondria-associated ER membrane; C: cytosol. DAVID Gene Ontology enrichment analysis of MS-identified proteins. The most enriched (top 10) biological pathways (**C**), cellular components (**D**), and molecular functions (**E**) of the ranked protein list. (**F**) KEGG pathway enrichment analysis of MS-identified proteins.

A PPI network analysis showed that interactions between proteins related to carbohydrate metabolism were evident (e.g., Dld, Pdhb, Pkm, Gapdh, Idh3g, Pdk1, and Slc25a11) in the PSD:ZDF group. Additionally, interactions among oxidative phosphorylation-related proteins were found both in the PSD:ZDF (i.e., Ndufv1, Ndufa11, COX2, Atp5l, and ND2) and the PDZ:PSD (i.e., ND2, Ndufb6, and Atp5l) groups (Figure 8A, 8B).

The DEPs were classified into 22 pathways in the PSD:ZDF group and five pathways in the PDZ:PSD groups. In the PSD:ZDF group, KEGG pathway annotation revealed a strong enrichment of pathways such as Alzheimer's disease (AD) and oxidative phosphorylation (OXPHOS; Figure 8C). There were seven DEPs (i.e., Apoe, Ndufv1, Ndufa11, COX2, Gapdh, Mapk1, and Ppp3r1) observed in the AD pathway and five DEPs (i.e., Ndufv1, Ndufa11, COX2, Atp5l, and ND2) were observed in the OXPHOS pathway (Figure 8E, 8G). In the PDZ:PSD group, the AD pathway was also strongly enriched (Figure 3D). Furthermore, five DEPs (i.e., Lrp1, Apoe, Ndufb6, Gapdh, and Mapk1) were found in the AD pathway and three proteins (i.e., ND2, Ndufb6, and Atp5l) were found in the OXPHOS (Figure 8F, 8H).

Representative proteins differentially expressed in brain MAM

Based on the results of functional analysis, 11, 4, and 14 representative proteins in the PSD:ZDF, PDZ:PSD and PSD:ZDF/PDZ:PSD combined groups were selected for protein abundance analysis, respectively (Figure 9). The common proteins in both groups are the glycolysis/gluconeogenesis proteins Pkm and Gapdh, protein metabolism-related proteins Alg2 and Rab5c, lipid metabolism proteins Acot7, Abhd12, Apoe, and Fdxr, OXPHOS proteins Atp5l and ND2, and cytoskeletal and synaptic-related proteins OMG, Mapk1, Gng12, and Dbnl (Figure 9C).

Validation of selected DEPs by western blotting

To verify the quantitative results of the iTRAQ-LC/MS/MS experiments, western blotting experiments

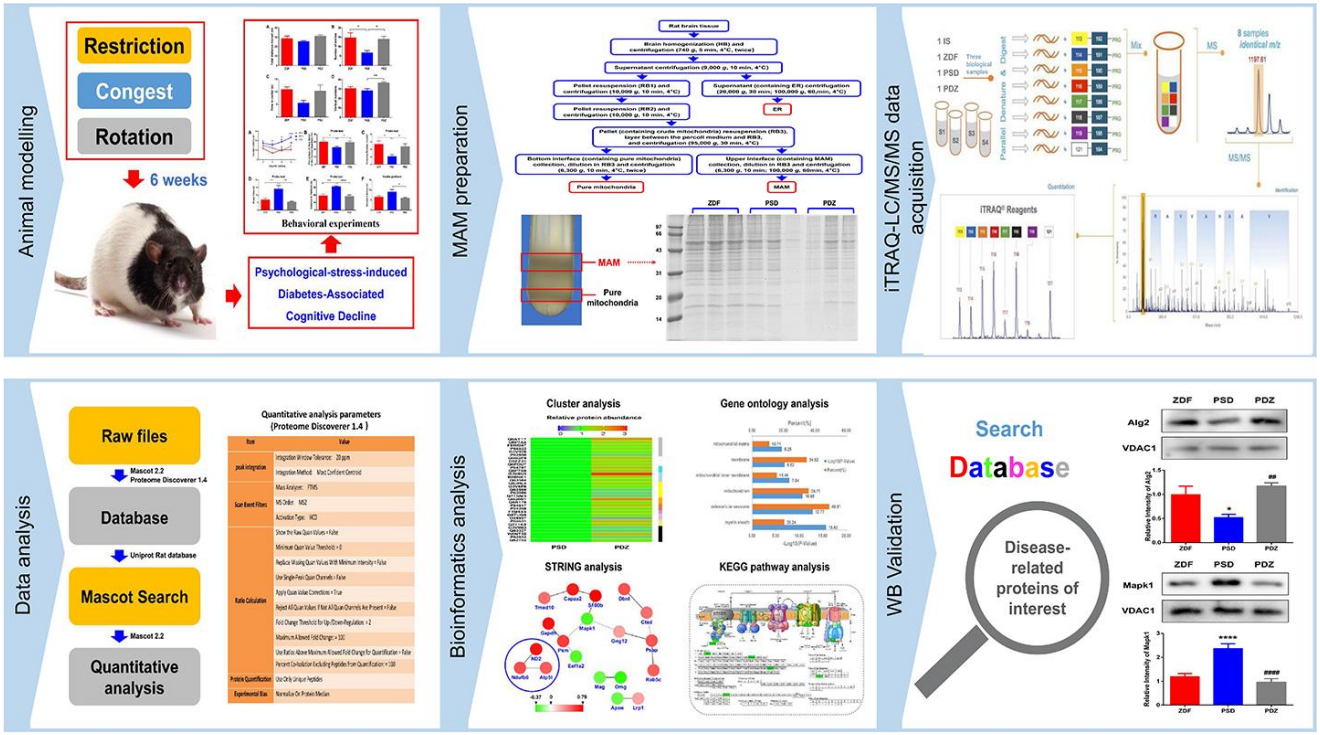

Figure 5. Proteomics workflow. An animal model of PS-induced diabetes-associated cognitive decline was established by exposure to three chronic psychological stressors. Fresh brain tissue MAM was extracted using gradient centrifugation, sample lysis was performed, and proteins were detected by an iTRAQ 8-plex. Following digestion and labelling, the samples were pooled, the peptides were fractionated by EASY-nLC1000 chromatography, and fractions were subsequently analyzed by standard LC-MS/MS. Peptides were identified and quantified based on their iTRAQ reporter area and relative protein quantification was inferred from these values. Key proteins were screened based on bioinformatics analysis and public databases were searched to further screen for differentially expressed proteins closely related to disease, for validation.

were performed on five selected DEPs (Apoe, Mapk1, Pkm, Gapdh, and Alg2). There were significantly increased levels of Apoe and Mapk1 in PSD:ZDF rats (Figure 10A, 10B) and significantly decreased levels in PDZ:PSD rats. These experiments also demonstrated that Pkm, Gapdh, and Alg2 expression was decreased sharply in the PSD:ZDF group and that ZBPYR treatment enhanced their expression (Figure 10C–10E).

DISCUSSION

Chronic PS as a common factor in modern life increases the risk of T2DM, but its pathogenesis in T2DM and DACD, generally considered to be a CNS complication of diabetes, is still unclear. In current study, a proteomic analysis on brain MAM samples was adopted to identify protein expression differences in animals with PSD and

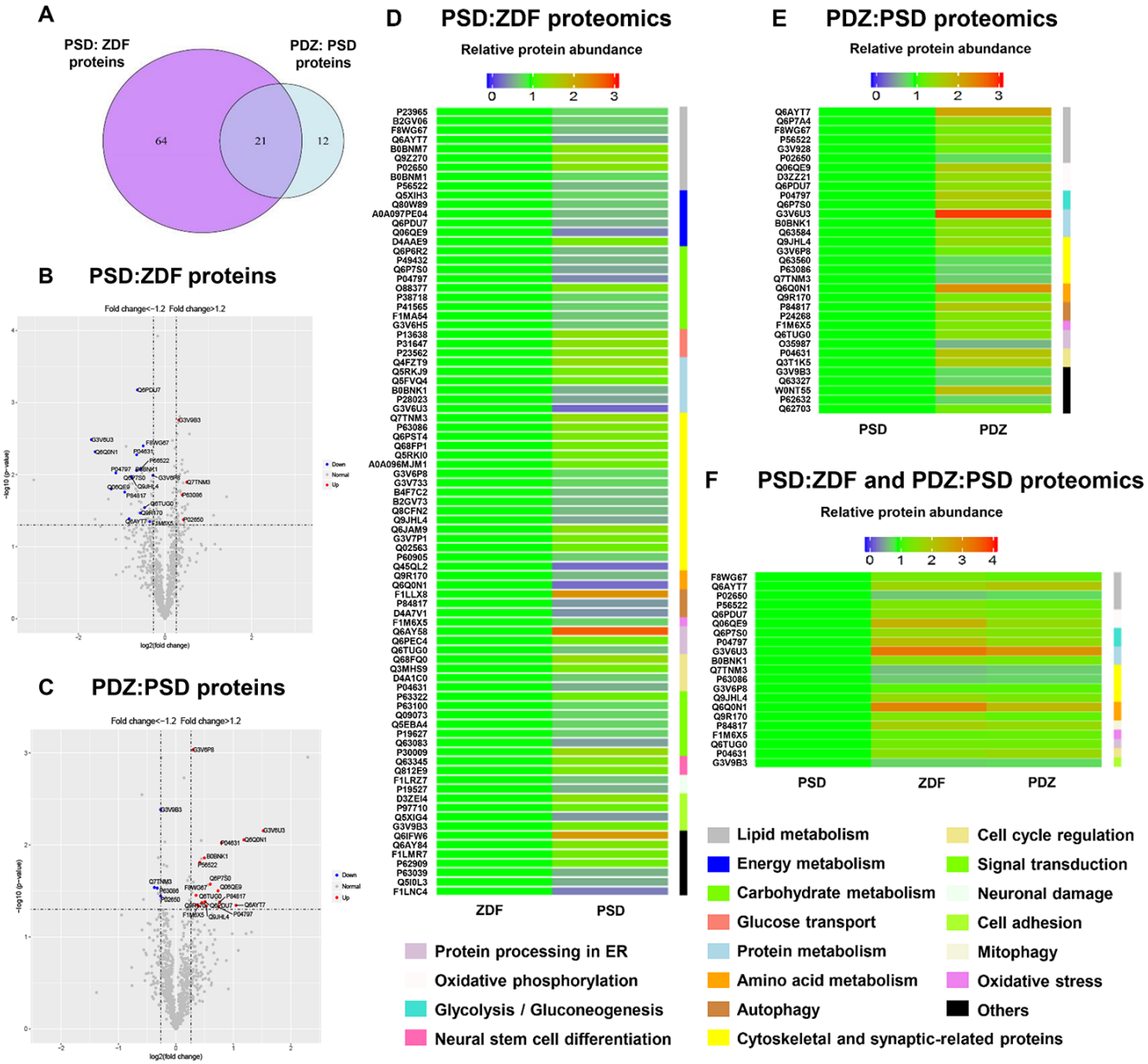

Figure 6. Analysis and comparison of the brain MAM proteins between PSD:ZDF and PDZ:PSD groups. (**A**) Using a fold change cutoff of ≥1.2 and a p-value cutoff of ≤0.05, a Venn diagram was constructed to find differentially regulated proteins in the PSD:ZDF, PDZ:PSD, or both. Volcano plots showing log2 fold-change (x-axis) and -log10 p-value (y-axis) were used for all quantified proteins in the PSD:ZDF (**B**) or PDZ:PSD group (**C**). Colored dots indicate proteins commonly expressed in both groups and the upregulated and downregulated proteins are labeled by red and blue, respectively. (**D**, **E**) Chronic PS caused 85 differentially expressed proteins and ZBPYR treatment resulted in 33 proteins to be differentially expressed. (**F**) Twenty-one overlapped proteins were differentially expressed in both groups (n=3 per group).

also to assess the effects of ZBPYR on PSD. We used male Zuker diabetes fatty (ZDF) rat as T2DM model, which is initiated with a mutation in the leptin receptor gene. When fed with a diet of Purina 5008, the ZDF rats exhibit the following characteristics: hyperglycemia, which develops between 7 and 10 weeks of age; early hyperinsulinemia, which rapidly falls as the beta cells fail; Insulin resistance and abnormal glucose tolerance, which becomes progressively worse with age; and spatial cognitive impairment, which occurs at 16 weeks of age.

Chronic PS aggravates diabetes and cognitive impairment

High concentrations of GCs enhance the risk of developing T2DM by increasing hepatic glucose production and reducing insulin secretion and sensitivity [11], while also increasing the risk of cognitive impairment through hippocampal neuronal loss, decreased neurogenesis, and dendritic atrophy [12]. In the current study, PSD rats demonstrated an increasing trend in blood

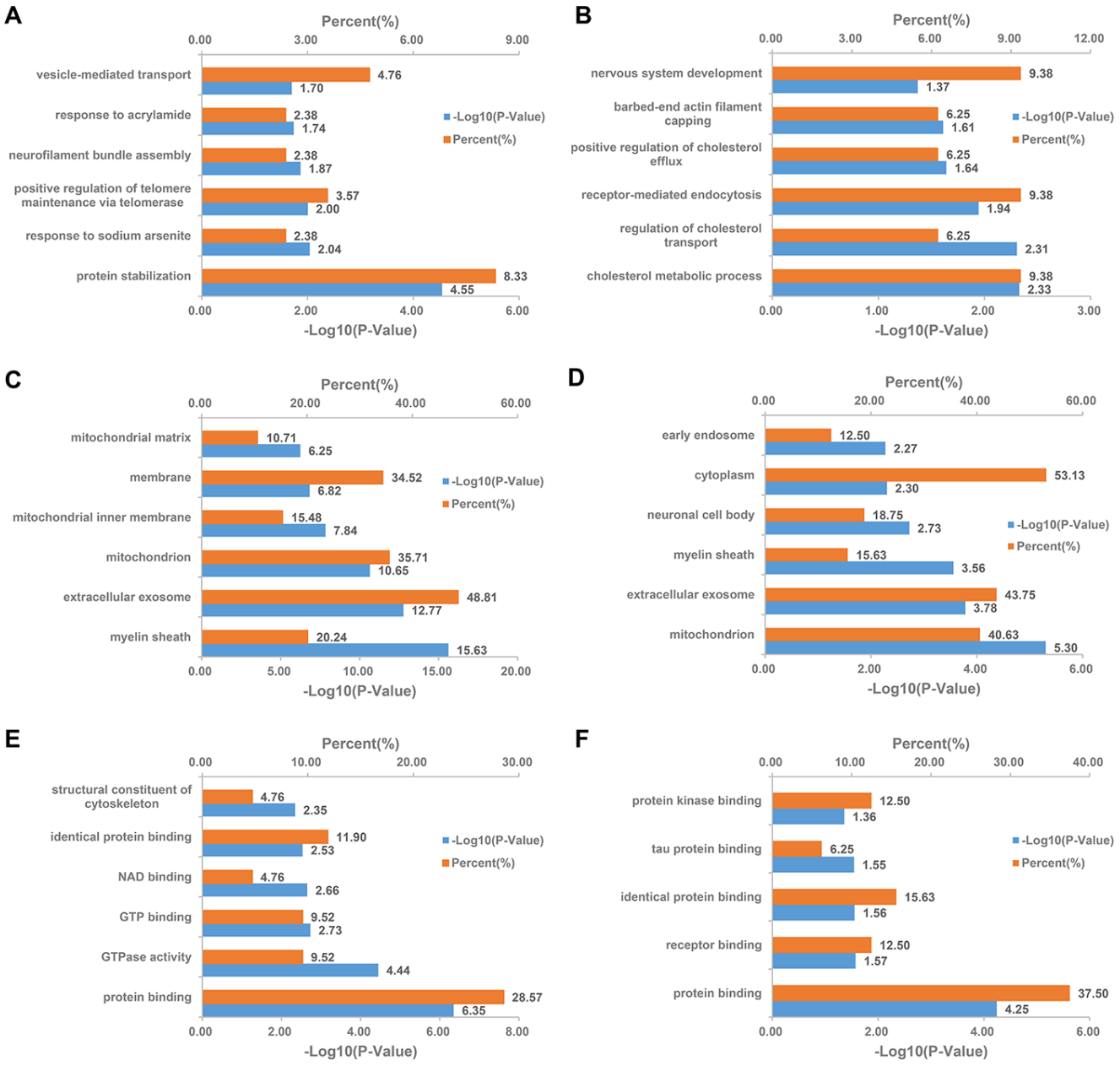

Figure 7. DAVID Gene Ontology enrichment analysis for the differentially expressed MAM proteins in PSD and PDZ rats. Enrichment analysis for MAM proteomics in the PSD:ZDF group by biological processes (**A**), cellular component (**C**), and molecular function (**E**), respectively. Enrichment analysis for MAM proteomics in the PDZ:PSD group by biological processes (**B**), cellular component (**D**), and molecular function (**F**), respectively.

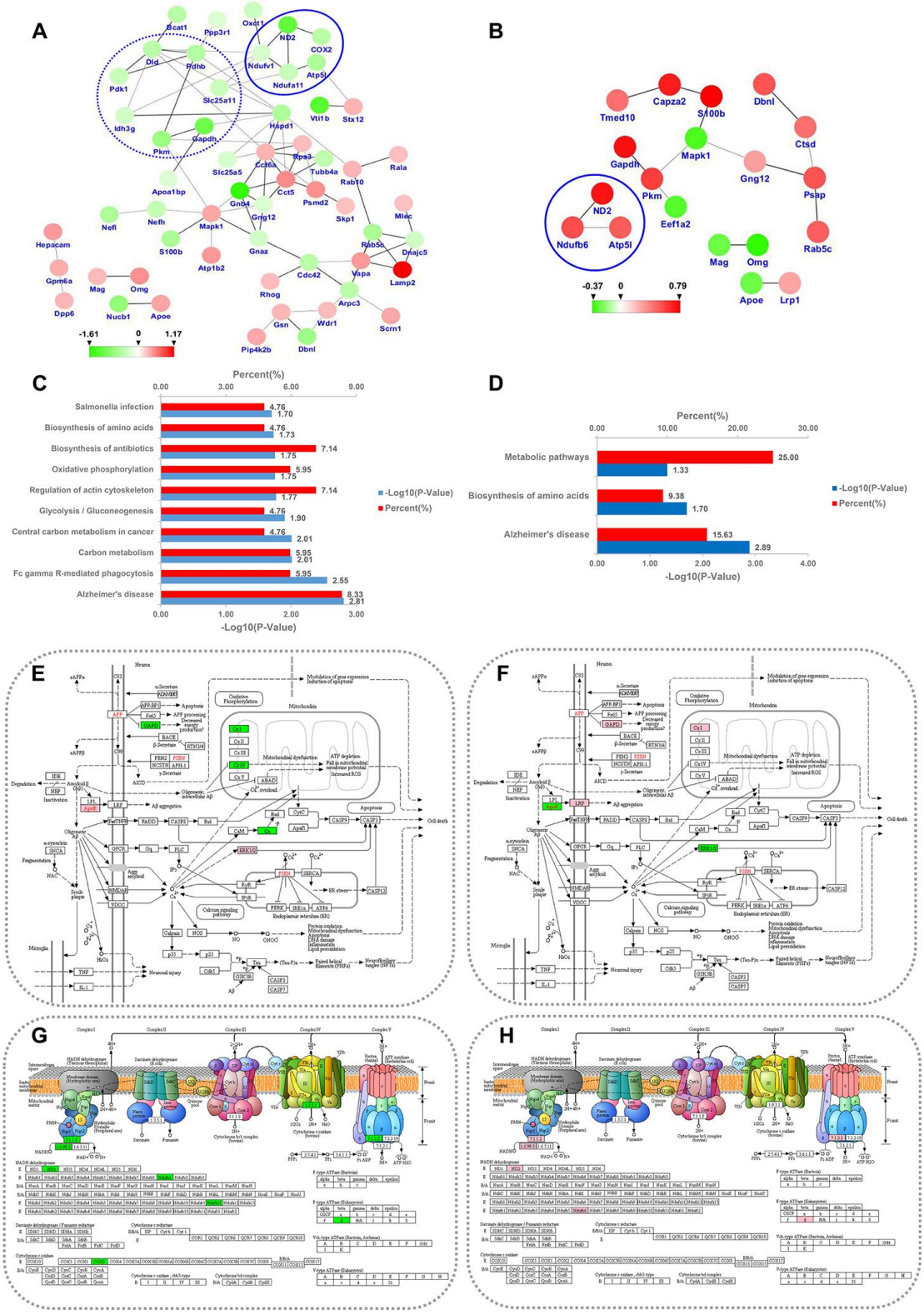

Figure 8. PPI network and KEGG pathway analysis for the differentially expressed MAM proteins in PSD and PDZ rats. Intricate PPI networks among the differential proteins in the PSD:ZDF (**A**) and PDZ:PSD (**B**) groups. Balls represent proteins, some of which are increased (red balls), others decreased (green balls). KEGG pathway enrichment analysis for differential proteins in the PSD:ZDF (**C**) and PDZ:PSD (**D**) rats. Alzheimer's disease pathway map in PSD:ZDF (**E**) and PDZ:PSD (**F**) rats, respectively. Oxidative phosphorylation pathway map in PSD:ZDF (**G**) and PDZ:PSD (**H**) rats, respectively. The upregulated and downregulated proteins are labeled in pink and green, respectively.

glucose levels, sustained activation of the HPA axis, and both behavioral and cognitive anomalies. These changes were associated with 85 MAM proteins that were significantly modulated in the brains of PSD rats. Bioinformatics analyses demonstrated that the modulated proteins were involved in OXPHOS, glycolysis/gluconeogenesis, synaptic function, protein metabolism, lipid metabolism, cytoskeleton, glucose transport, and calcium signaling. Additionally, the current study suggests that elevations in CORT and ACTH occur prior to the development of glucose intolerance and may facilitate the succeeding onset of hyperglycemia in ZDF rats. Average blood glucose levels in PSD rats reached diabetes levels (blood glucose ≥ 16.7 mmol/L) at eight weeks of age, while ZDF rats did not meet this level (PSD: 17.34 ± 1.63 vs. ZDF: 15.26 ± 1.04 mmol/L). At nine weeks of age, the mean blood glucose levels in both groups exceeded 16.7 mmol/L (PSD: 22.76 ± 1.26; ZDF: 18.81 ± 0.94 mmol/L).

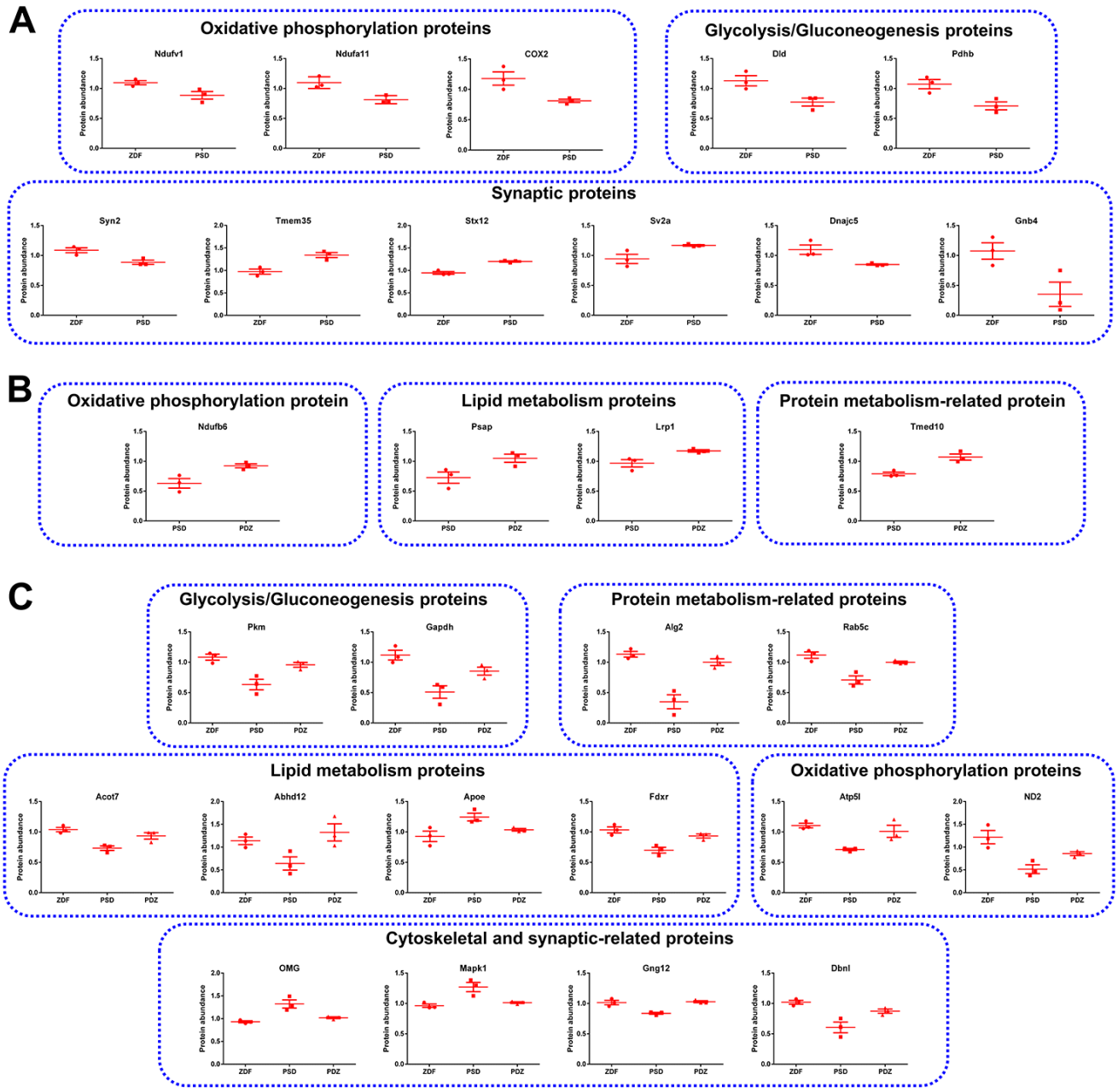

Figure 9. Representative MAM proteins that were differentially expressed in PSD and PDZ rats. (**A**) Proteins that were abnormally expressed in PSD rats. (**B**) Proteins that were differentially expressed in PDZ rats. (**C**) MAM proteins that were differentially expressed in both PSD and PDZ rats (mean ± SEM, n=3 per group).

ZBPYR treatment alleviates diabetes and cognitive impairment

A previous study conducted by our research group showed that the benefit of ZBPYR on DACD may be achieved through improvements in dendritic spine density, reduction of $A\beta_{1-42}$ deposition, attenuation of brain leptin and insulin signaling pathway injury, and maintenance of gut microbiota homeostasis. In the current study, ZBPYR significantly improved the chronic activation of the HPA axis, reduced blood glucose concentrations, promoted insulin sensitivity, slowed the progression of diabetes, as well as enhanced exploratory behavior, learning, and memory performance in PSD rats. These changes were associated with 33 MAM proteins that were significantly modulated in the brains of PDZ rats. Bioinformatics analyses showed that the modulated proteins were involved in OXPHOS, glycolysis/gluconeogenesis, synaptic function, protein metabolism, lipid metabolism, and protein processing in the ER.

Chronic PS and ZBPYR treatment result in the common differential expression of brain MAM proteins in ZDF and PSD rats

Energy metabolism

Chronic PS is associated with abnormal energy metabolism [13]. In the current study, four proteins associated with energy metabolism, namely Gapdh, Pkm, Atp5l, and ND2 were downregulated in the PSD group. The inhibition of Gapdh activity can contribute to apoptosis, a common phenomenon in cognitive impairment, including in AD, through the glycolytic

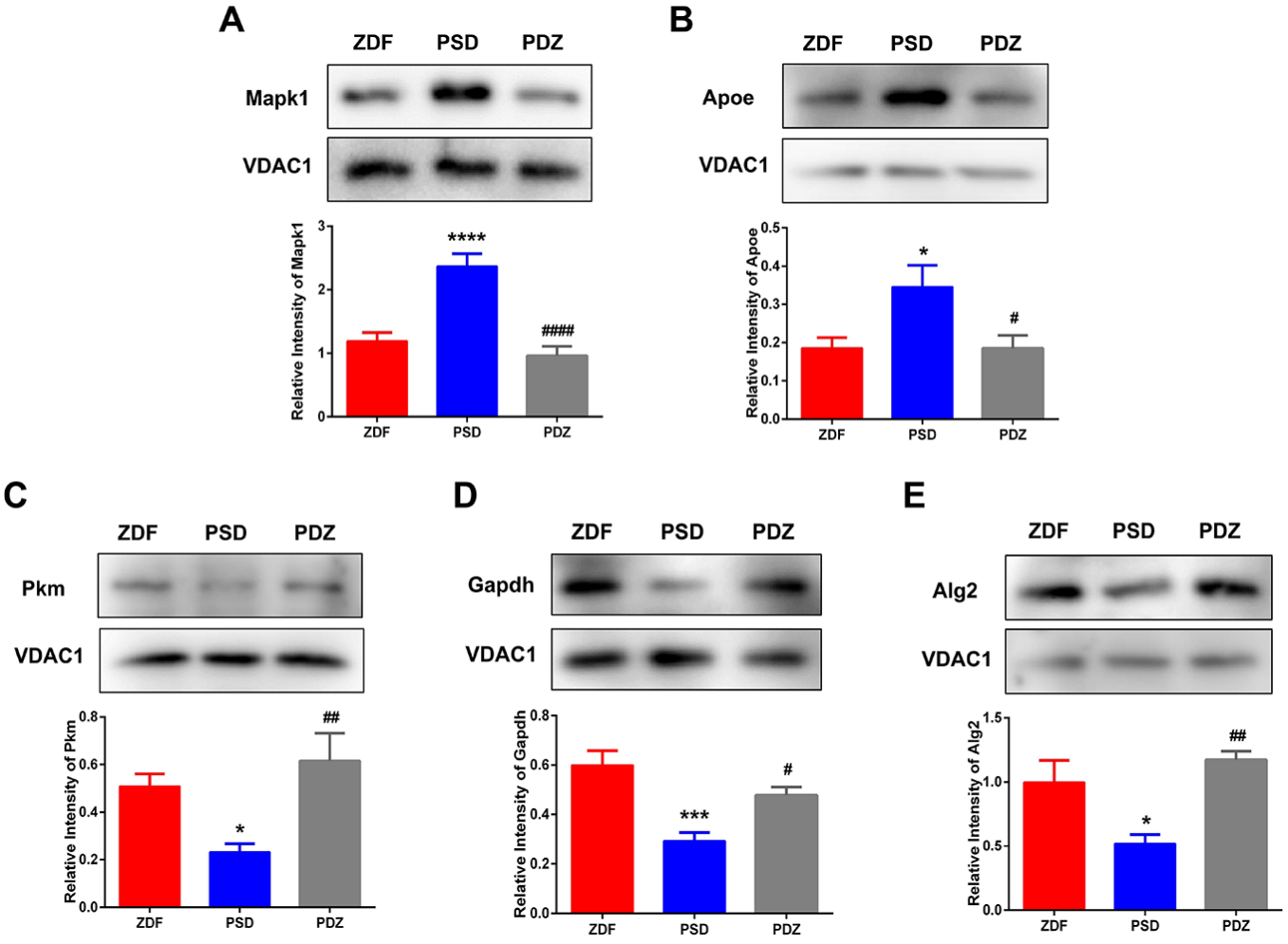

Figure 10. Western blotting analysis for selected differentially expressed proteins. MAM fractions from ZDF, PSD, and PDZ rats were analyzed by western blotting using antibodies against mitogen-activated protein kinase 1 (Mapk1) (**A**), apolipoprotein E (Apoe) (**B**), pyruvate kinase (Pkm) (**C**), glyceraldehyde-3-phosphate dehydrogenase (Gapdh) (**D**), and ALG2, alpha-1,3/1,6-mannosyltransferase (Alg2) (**E**). VDAC1 was used to ensure equal protein loading and transfer. The levels of Pkm, Mapk1, Apoe, Gapdh, and Alg2 were normalized relative to VDAC1 levels. $^{*}p$ <0.05, $^{***}p$ <0.001, $^{****}p$ <0.0001 PSD vs. ZDF; $^{\#}p$ <0.05, $^{\#\#}p$ <0.01, $^{\#\#\#\#}p$ <0.0001 (mean ± SEM, n=3 per group).

generation of toxic side-products [14]. PKM plays a prominent role in the maintenance of different forms of persistent, long-term synaptic plasticity [15] and is used as a biomarker for detecting disease progression and therapeutic response in AD [16]. ATP5L is downregulated in the choroid plexus in those with AD, while reduced choroid plexus function impaired the clearance of toxic metabolites and may facilitate neuronal death during AD progression [17]. ND2 is the core component of mitochondrial respiratory chain complex I. Previous studies have shown that mRNA levels of mitochondrial genome-encoded COX I is significantly decreased in the temporal cortex in those with AD [18]. The levels of these four proteins were upregulated in the PDZ group, suggesting that ZBPYR improved PSD, potentially by regulating energy metabolism, including glycolysis and OXPHOS.

Lipid metabolism

Chronic PS has been shown to affect lipid metabolism [19]. In the current study, chronic PS caused a simultaneous decrease of Acot7 and Abhd12 in the PSD group, but increased Apoe. Apoe plays an important role in lipid transport in the central nervous system, regulating neuronal survival and sprouting [20]. Genome-wide association studies have confirmed that APOE gene polymorphisms are closely linked to the risk of AD and the APOE ε4 allele is the strongest genetic risk factor for AD [21]. Acot7 is highly expressed in neurons, counter-regulates fatty acid metabolism in neurons, and protects against neurotoxicity [22]. In line with this, Acot7N$^{-/-}$ mice exhibit neurological dysfunction and neuro-degeneration. Abhd12 is an enzyme that catalyzes the hydrolysis of 2-arachidonoyl glycerol (2-AG). Furthermore, 2-AG regulates neurotransmission and neuroinflammation [23]. The pathological processes of many diseases are connected with inflammation, including DM and cognitive impairment. Given that expression changes of three proteins in the PSD group was the inverse of that in the PDZ group, alternated protein expression affecting lipid metabolism is plausibly a common phenomenon observed in animals with cognitive dysfunction.

Protein metabolism

Chronic PS has been demonstrated to affect protein metabolism [24]. Changes in protein metabolism are essential to disease onset and progression in many neurodegenerative diseases, such as AD [25]. In the current study, the levels of Alg2 and Rab5c were decreased in the PSD group, while their levels were elevated in the PDZ group. Alg2 acts as an alpha-1,3 mannosyltransferase. Defects in this gene have been associated with the congenital disorder of glycosylation type Ih, which results in a wide variety of clinical features such as defects in nervous system development. Rab5c is a small GTPase of the Ras superfamily. Higher Aβ production has also been observed in Rab5-endocytic vesicles in the early endosome and lysosomes in the brain of those with AD, whereas silencing of only the Rab5C isoform significantly increases APP, soluble APP, and $A\beta_{42}$ levels [26]. The current results suggest that ZBPYR improved PSD potentially by regulating protein metabolism, including post-translational modifications.

Synaptic dysfunction

A high level of glucocorticoids, induced by chronic stress, causes specific synaptic deficits in the hippocampus, accompanied by stress-induced behavioral dysfunction [27]. In the current study, chronic PS indeed caused synaptic dysfunction with increased levels of Mapk1, OMG, and Gng12 and decreased Dbnl levels, while ZPBYR treatment stabilized their expressions. MAPK1 plays a key role in cellular proliferation and differentiation during neural development, as well as in cognition and memory formation [28]. Moreover, the expression of MAPK1 is significantly upregulated in the brains of AD patients and in rodent models [29], leading to synaptic plasticity damage and impairment of learning and memory capacity. OMG is a myelin-associated inhibitor (MAI). MAIs stabilize synaptic ultrastructures by modulating cytoskeletal rearrangements and suppressing activity- and experience-dependent synaptic plasticity [30]. Furthermore, increased MAI expression is implicated in a number of neurological conditions, including AD. Gng12 is known as the γ12 subunit of G proteins. Results from one functional gene group approach suggest that the involvement of synaptic heterotrimeric G proteins in cognitive ability and alterations in synaptic signaling processes could explain this correlation [31]. Taken together, these findings suggest that ZPBYR treatment improves PSD plausibly by regulating the synaptic dysfunction associated with the alternated protein expression of Mapk1, OMG, Gng12, and Dbnl.

Chronic PS leads to specific changes in brain MAM proteins in ZDF rats

Calcium signaling

Voltage gated Ca^{2+} channels are among the most pronounced targets of corticosteroid hormones. Deregulation of intracellular calcium signaling has been implicated in the pathogenesis of AD. In the current study, chronic PS caused a simultaneous decrease in Ppp3r1, Slc25a5, Nipsnap1, and Nucb1 in the PSD group. Ppp3r1 encodes a regulatory subunit of calcineurin. In animal models, the disruption of calcineurin activity has severe effects on memory [32]. Furthermore, a genetic variant of Ppp3r1 is strongly associated with the rapid progression of AD in humans

[33]. Slc25a5 and Nipsnap1 play prominent roles in signal transduction and postsynaptic density function regulation [34, 35], therefore, the abnormal expression of these genes can result in memory impairment. Nucb1 inhibits the aggregation of islet-amyloid polypeptide associated with T2DM, and $A\beta_{42}$ associated with AD by stabilizing their respective protofibril intermediates [36]. In post-mortem brains of AD patients, NUCB1 protein levels have been found to be reduced by an average of 50% compared to controls. The current results demonstrate that decreased protein expression of the calcium signaling pathway could plausibly contribute to DACD.

ZBPYR treatment causes specific changes of brain MAM proteins in PSD rats

Autophagy

The current results also showed that an autophagy-related protein, Ctsd, was upregulated in the PDZ group. Ctsd, a lysosomal protease, is involved in the degradation of the APP protein, the processing of Aβ

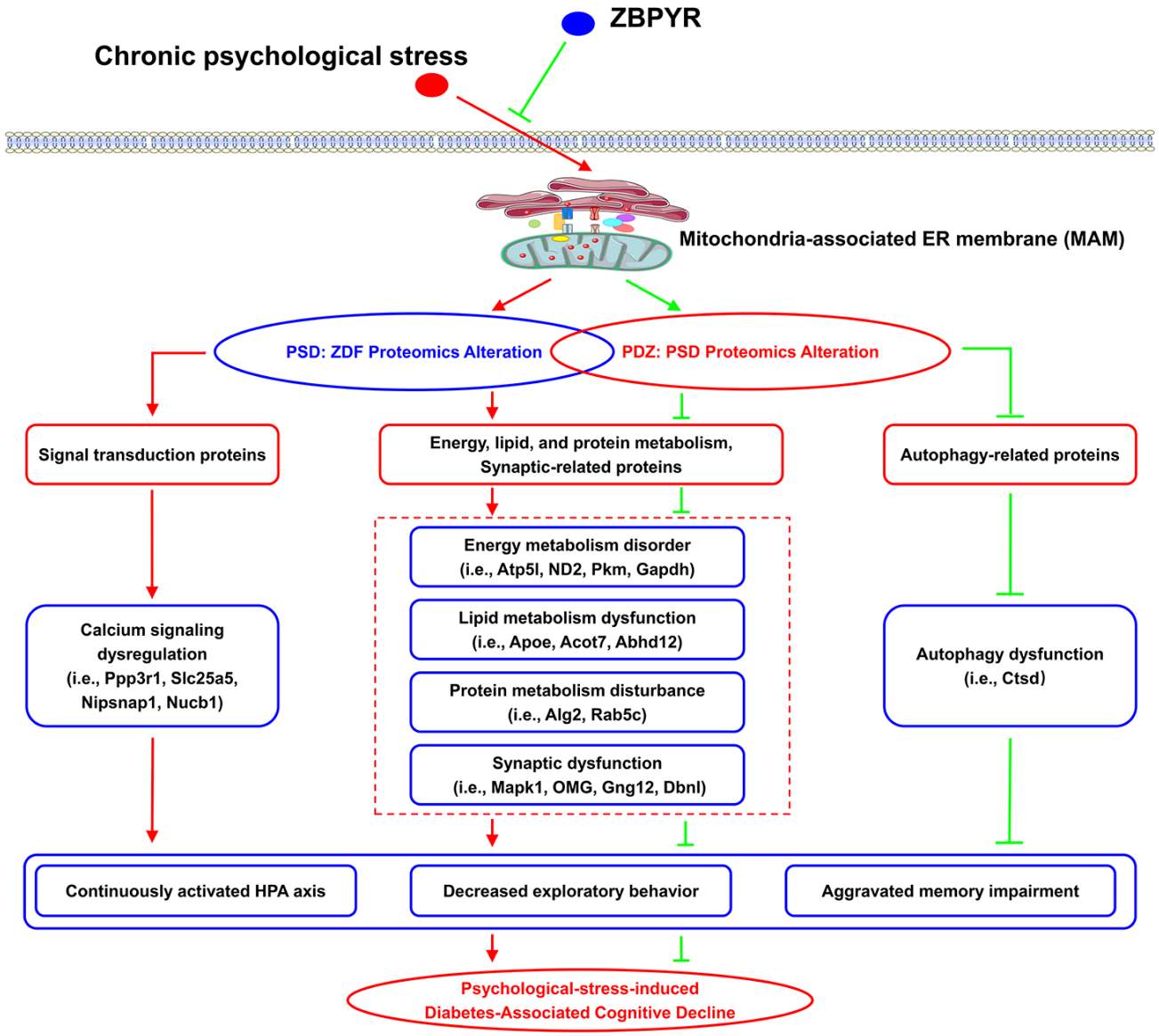

Figure 11. The potential mechanism of chronic PS and ZBPYR treatment. Chronic PS causes proteomic alterations in brain MAM of ZDF rats, including in proteins related to lipid and protein metabolism, energy metabolism, synaptic function, and calcium signaling. ZBPYR treatment results in proteomic alterations in PSD rats, including in proteins related to lipid and protein metabolism, energy metabolism, synaptic function, and autophagy. This may trigger the molecular basis of chronic PS aggravated diabetes-associated cognitive decline (i.e., persistent hyperactivity of the HPA axis, decreased exploratory behavior, and aggravated memory impairment) and provides a potential therapeutic mechanism of ZPBYR.

peptides and tau, and the clearance of amyloid plaques *in vitro* [37–39]. Consistent with previous results, our research group has previously shown that ZBPYR treatment improves Spleen-yin deficiency DACD by promoting the occurrence of autophagy [40]. Therefore, we have reason to believe that ZBPYR improved DACD potentially by influencing autophagy, and that Ctsd may be a molecular target of the neuroprotective effects of ZBPYR.

Regulation of signaling pathways enriched in DEP datasets

Alzheimer's disease (AD) pathway

The current data suggested that two upregulated DEPs (Apoe and Mapk1) and five downregulated DEPs (Ndufv1, Ndufa11, COX2, Gapdh, and Ppp3r1) were involved in Alzheimer's disease signaling in the PSD:ZDF group, while three upregulated DEPs (Lrp1, Ndufb6, and Gapdh) and two downregulated DEPs (Apoe and Mapk1) were observed in the PDZ:PSD group. Alzheimer's disease pathway maps showed that chronic PS may result in Aβ aggregation, mitochondrial dysfunction, decreased energy production, and apoptosis, while ZBPYR administration could improve above dysfunction. Alzheimer's disease (AD) is a chronic disorder that slowly destroys neurons and causes serious cognitive disability. It is also associated with senile plaques and neurofibrillary tangles. Similarly, clinical studies have shown that amyloid plaques and neurofibrillary tangles are present in the brain tissue of patients with T2DM and the density of amyloid plaques is closely related to the course of T2DM [41]. Consistent with this, animal experiments have confirmed that diabetic mice not only have learning and memory dysfunction, but that their brain neurons have AD-specific pathological changes [42]. Our proteomics data is partially consistent with this mechanism, suggesting that ZPBYR treatment improved PSD potentially by regulating the abnormal protein expression of the Alzheimer's disease pathway.

Oxidative phosphorylation (OXPHOS) pathway

We also found that five downregulated DEPs (Ndufv1, Ndufa11, COX2, Atp5l, and ND2) and three upregulated DEPs (ND2, Ndufb6, and Atp5l) were involved in Oxidative phosphorylation signaling in the PSD:ZDF and PDZ:PSD groups, respectively. Given that expression change in the PSD:ZDF group was opposite of that in the PDZ:PSD group, it follows that chronic PS and ZBPYR administration may interfere with the coordination of energy protein mechanism (gene/protein expression) in MAM among the two groups. Oxidative phosphorylation is a way for mitochondria to supply energy metabolism when sufficient oxygen is provided. Mitochondrial dysfunction primarily manifests as disordered energy metabolism, perturbations in the electron transport chain, synaptic dysfunction, and neuronal apoptosis. Energy metabolism disorder has been demonstrated in brain injury caused by diabetes. Clinical trials and animal studies have shown that the activity of mitochondrial complex I-IV in the brain of those with AD decreased when accompanied with abnormal oxygen consumption [43, 44]. Additionally, a previous proteomic study from our research group demonstrated that several molecules closely related to energy metabolism changed in the hippocampus of the DACD model rats, suggesting a possible energy metabolism disorder in the model rat [45]. Collectively, this evidence points to the notion that perturbations of mitochondrial energy metabolism-related proteins responsible for ATP generation via oxidation phosphorylation play an important, perhaps crucial, role in the development of DACD and treatment of ZBPYR.

Study advantages and limitations

Compared with previous studies, the merits of this work could be summarized by four characteristics, including the closer animal model to the pathogenesis of DACD in humans, the more sophisticated proteomic technique, the more precise subjects—MAM fractions from brain, and stress stimulation with reduced potential adaptability. First, ZDF rat has been used as a classic model to study the pathogenesis of T2DM caused by obesity and insulin resistance and it has been shown to have spatial cognitive impairment by 16 weeks of age. In other words, the ZDF rat is a promising animal model by which to study DACD. Furthermore, almost all of previous studies have focused on the MAM profiles of the mouse with normal physiological and disease states [5, 6, 46], while there are currently no studies focused on the effects of psychological stress and drug administration on the rat MAM proteome. Therefore, we chose ZDF rats as the research objects. Second, a number of previous studies have analyzed proteins in the MAM fraction using different proteomics techniques, such as one-dimensional gel electrophoresis, label-free, and iTRAQ-labeled technology combined with LC-MS/MS [5, 47, 48]. Based on the above background, we selected the more sophisticated and sensitive proteomics approach, namely iTRAQ-based LC-MS/MS, to reveal protein changes. Third, many proteomics studies have been performed at the levels of the whole cell or tissue lysates. It may be better to understand the essential regulation mechanisms and biological functions of MAM with a spatio-temporal resolution through subcellular fractionation. It is of importance to note that since MAM is a hub for both neurodegeneration and metabolic disease, it is useful to select brain MAM for further proteomics research to understand the

pathogenesis of PSD and the mechanism of ZPBYR. Finally, chronic PS exposure is defined as a prolonged period of stress, during which an animal is exposed to a continuous or repeated psychological stressor without habituation. Habituation, however, can be very hard to predict given that it depends on the interval between stressors as well as the intensity, duration, predictability, and types of stressors used. Therefore, by observing physical status and indicators of rats, we continuously adjusted the interval and duration of stress intervention to minimize the possibility of adaptation or habituation.

However, there are also limitations to the chosen study design. First, although animal models are essential to preclinical trials, substantial work is needed in preclinical and human studies to fully illustrate the effects of PS and ZBPYR on patients with T2DM and DACD. Additionally, due to the particularity of the strain, the current study was restricted to male ZDF rats; however, we cannot exclude that the protein profiles may differ in female animals. Indeed, studies have shown that gender differences in neuro-psychological endocrine activation make females more prone to the effects of long-term psychosocial stress on health [49]. Furthermore, although the current study has found common and specific differential proteins caused by PS and ZBPYR, the exact mechanisms by which this occurred could not be directly determined. In particular, there was a lack of evidence from animals with specific gene knockouts to determine whether the effects of the two interventions on lipid and protein metabolism, energy metabolism, synaptic function, autophagy, and calcium signaling pathways were direct effects or in association with a signaling cascade.

CONCLUSIONS

In summary, we demonstrated that chronic PS (restriction, rotation, and congestion) of ZDF rats perpetually interfered with the HPA axis, affected exploratory behaviors, and promoted cognitive anomalies, while ZBPYR treatment significantly improved the above interference. Additionally, elevations in stress-related indicators (i.e. CORT and ACTH) may facilitate the subsequent onset of hyperglycemia in ZDF rats. Proteomic analysis demonstrated that chronic PS is related to changes in the MAM proteome of ZDF rats, including proteins related to OXPHOS (Atp5l and ND2), glycolysis (GAPDH and PKM), lipid metabolism (Apoe, Acot7, and Abhd12), protein metabolism (Alg2 and Rab5c), and synaptic dysfunction (Mapk1, OMG, Gng12, and Dbnl). These proteins were also regulated by ZBPYR administration. Furthermore, calcium signaling and autophagy may play roles in the pathogenesis of PSD and the mechanisms of ZBPYR, respectively. Chronic PS as a common factor in modern life could therefore plausibly contribute to the evolution and progression of T2DM and DACD (Figure 11), while ZBPYR administration may significantly delay and alleviate the occurrence and progression of T2DM and DACD.

MATERIALS AND METHODS

Animals and treatment protocol

Male, 6-week-old, obese Zuker diabetic fatty (ZDF) rats were purchased from Vital River Laboratories (Beijing, China) and housed in a specific, pathogen-free animal experimental center in Nanjing University of Chinese Medicine. The animals were fed autoclaved Purina 5008 chow and water *ad libitum* and were housed at 24° C ± 2° C with 65% ± 5% humidity with a 12-hour light-dark cycle. All animal experiments were conducted in accordance with the National Institutes of Health Guide for the Care and Use of Laboratory Animals and were approved by the Animal Ethics Committee of Nanjing University of Chinese Medicine (Approval No. ACU170606).

After one week of acclimatization, the ZDF rats were randomly distributed into three groups (n=8 each): a ZDF control group, a PSD group, and a PDZ group. The PSD and PDZ groups were exposed to three stressful stimulations: restriction, rotation, and congestion all lasting for six weeks. The duration of the restricting stress experiment lasted for 1 hour in weeks 1-2, 1.5 hours in weeks 3-4, and 2 hours in weeks 5-6. The rotation and congestion procedures were performed as previously described in detail [50].

Preparation and administration of ZBPYR

ZBPYR, consisting of 12 crude herbs, was purchased from Nantong Sanyue Chinese Traditional Medicine Co., Ltd. (Nantong, China) and its preparation and administration was identical to that described in a previous study [50]. During weeks 8 to 15, ZBPYR was administered by oral gavage at a dose of 0.1 mL/10 g body weight to the PDZ group, while the PSD and control groups were administered with an equal dose of ultrapure water.

Random blood glucose test, oral glucose tolerance test, and insulin tolerance test

The RBG levels in blood samples were measured from weeks 7 to 15. Following chronic PS experiments, all rats were fasted for 14 hours (overnight, for the OGTT) and 6

hours (for the ITT). Blood was sampled at 0, 30, 60, 90, and 120 minutes following glucose (2 g/kg body weight) administration and at 0, 15, 30, 60, 90, and 120 minutes following insulin (0.5 U/kg body weight; Wanbang Biopharmaceuticals Co., Ltd., Xuzhou, China) injection. Blood glucose levels were all determined from tail blood.

Plasma ACTH and corticosterone assays

Tail blood samples were collected weekly. The samples were centrifuged at 1300×*g* for 10 minutes, and the supernatants were kept frozen at −80° C. Plasma concentrations of ACTH and CORT were measured using a Rat ACTH ELISA kit (Nanjing Jiancheng Bioengineering Institute, Nanjing, China) and a rat CORT ELISA kit (Nanjing Jiancheng Bioengineering Institute). The procedures were conducted in accordance with the instruction manuals, and the data were expressed as ng/ml.

Behavioral experiments

The OFT was performed during the first day and the MWM was performed during days 2-7 of the last seven days. All procedures were conducted as previously described in detail [50]. The spontaneous locomotor activities were recorded for the OFT. The MWM test consisted of 5-day training for the hidden platform test and the probe trial while the visible platform training was conducted on day seven.

Isolation of MAM from rat brains

The MAM was isolated according to an established protocol [10] with minor modifications. Briefly, tissues were manually homogenized on ice and nuclei and unbroken cells were pelleted by centrifugation. The supernatant was collected and centrifuged to separate the crude mitochondria from plasma membranes, lysosomes, microsomes, and ER fractions. After several washes, the crude mitochondrial fraction was suspended in 4 ml resuspending buffer III layered on top of 16 ml of a 30% Percoll medium and centrifuged at 95,000×*g* for 30 minutes. The MAM fraction and the pure mitochondrial fraction were separately extracted from the Percoll gradient and were further purified by centrifugation, to remove contaminants. All fractions were flash frozen by liquid nitrogen and preserved at −80° C until use.

Quantitative proteomic analysis

The iTRAQ quantitative proteomic analysis was performed on triplicate samples of rat brain MAMs and on three independent rat brain MAM protein extractions per group, as described in the Supplementary Materials. After acquiring MS/MS data with a Q-Exactive (Thermo Finnigan, San Jose, CA, USA) mass spectrometer, all data files were processed using the Mascot 2.2 and Proteome Discoverer 1.4 (Thermo) to identify the peptides. The search parameters are detailed in the supplementary materials. All reported data were based on 99% confidence for peptide identification, as determined by a false discovery rate (FDR) of no more than 1%. Protein identification was supported by at least one unique peptide identification. Proteins with relative quantification p-values <0.05 and fold changes >1.2 were considered as significant.

Bioinformatics analysis

The DAVID bioinformatics resource (v6.8) (https://david.ncifcrf.gov/) was used for the GO annotation and KEGG pathway enrichment analysis. STRING (Search Tool for the Retrieval of Interacting Genes/Proteins) database version 11.0 (https://string-db.org/) was used to search for the protein-protein interaction (PPI) networks of the differently regulated proteins. The STRING-generated network was visualized and edited in Cytoscape version 3.7.1. Additionally, R (v3.5.2) was used to generate a Venn diagram and volcano plots to perform the logistic analysis on the MAM proteome.

Western blot analysis

Samples were lysed in a radio immunoprecipitation assay (RIPA) buffer (Beyotime, China) with a protease and phosphatase inhibitor cocktail (Cell Signaling Technology, USA). The protein samples, measured by a BCA protein assay kit (Beyotime, China), were loaded and resolved by SDS-PAGE, followed by electro-blotting onto the PVDF membranes. The membranes were probed with primary antibodies listed in Supplementary Table 5 and the corresponding HRP-conjugated secondary antibodies. The membranes were developed with an ECL kit (Tanon, China) using an Amersham Imager 600 (General Electric Company, USA).

Statistical analysis

The data are expressed as means ± standard error (SEM) and analyzed using GraphPad Prism 6.0 statistical software (GraphPad Software, USA). Statistical analyses were performed using Student's *t* tests for comparing two groups and one-way ANOVAs with Tukey's *post hoc* test for the comparison of three groups. Learning curves were analyzed by two-way repeated-measure ANOVAs and Bonferroni's multiple comparisons *post hoc* tests. The difference was considered to be statistically significant when $p \leq 0.05$.

AUTHOR CONTRIBUTIONS

L. B. Z and X. G. L conceived the concept, directed the project, designed the experiments, critically revised the manuscript, and was responsible for its financial supports and the corresponding works. H. Y. X, W. Z, H. S, and L. J. Z performed the experiments, obtained the samples, and acquired the data. H. Y. X and C. Y. Z prepared figures and tables. H. Y. X performed bioinformatic analysis and wrote the manuscript. All authors approved the final manuscript.

ACKNOWLEDGMENTS

The authors are grateful to the Shanghai Applied Protein Technology Co. Ltd. (Shanghai, China) for assistance with LC-MS/MS analysis.

CONFLICTS OF INTEREST

The authors declare that they have no conflicts of interest.

FUNDING

This work was supported by the Key Project of the National Natural Science Foundation of China (No. 81230084, 81730111), A Project Funded by the Priority Academic Program Development of Jiangsu Higher Education Institutions (Integration of Chinese and Western Medicine) and the Postgraduate Research & Practice Innovation Program of Jiangsu Province (No. KYCX18_1560).

REFERENCES

1. Kelly SJ, Ismail M. Stress and type 2 diabetes: a review of how stress contributes to the development of type 2 diabetes. Annu Rev Public Health. 2015; 36:441–62. https://doi.org/10.1146/annurev-publhealth-031914-122921 PMID:25581145

2. McCrimmon RJ, Ryan CM, Frier BM. Diabetes and cognitive dysfunction. Lancet. 2012; 379:2291–99. https://doi.org/10.1016/S0140-6736(12)60360-2 PMID:22683129

3. Umegaki H. Type 2 diabetes as a risk factor for cognitive impairment: current insights. Clin Interv Aging. 2014; 9:1011–19. https://doi.org/10.2147/CIA.S48926 PMID:25061284

4. Krols M, van Isterdael G, Asselbergh B, Kremer A, Lippens S, Timmerman V, Janssens S. Mitochondria-associated membranes as hubs for neurodegeneration. Acta Neuropathol. 2016; 131:505–23. https://doi.org/10.1007/s00401-015-1528-7 PMID:26744348

5. Völgyi K, Badics K, Sialana FJ, Gulyássy P, Udvari EB, Kis V, Drahos L, Lubec G, Kékesi KA, Juhász G. Early presymptomatic changes in the proteome of mitochondria-associated membrane in the APP/PS1 mouse model of Alzheimer's disease. Mol Neurobiol. 2018; 55:7839–57. https://doi.org/10.1007/s12035-018-0955-6 PMID:29468564

6. Wang X, Wen Y, Dong J, Cao C, Yuan S. Systematic in-depth proteomic analysis of mitochondria-associated endoplasmic reticulum membranes in mouse and human testes. Proteomics. 2018; 18:e1700478. https://doi.org/10.1002/pmic.201700478 PMID:29785746

7. Theurey P, Rieusset J. Mitochondria-associated membranes response to nutrient availability and role in metabolic diseases. Trends Endocrinol Metab. 2017; 28:32–45. https://doi.org/10.1016/j.tem.2016.09.002 PMID:27670636

8. Chen J, Liang L, Zhan L, Zhou Y, Zheng L, Sun X, Gong J, Sui H, Jiang R, Zhang F, Zhang L. ZiBuPiYin recipe protects db/db mice from diabetes-associated cognitive decline through improving multiple pathological changes. PLoS One. 2014; 9:e91680. https://doi.org/10.1371/journal.pone.0091680 PMID:24614172

9. Arruda AP, Pers BM, Parlakgül G, Güney E, Inouye K, Hotamisligil GS. Chronic enrichment of hepatic endoplasmic reticulum-mitochondria contact leads to mitochondrial dysfunction in obesity. Nat Med. 2014; 20:1427–35. https://doi.org/10.1038/nm.3735 PMID:25419710

10. Wieckowski MR, Giorgi C, Lebiedzinska M, Duszynski J, Pinton P. Isolation of mitochondria-associated membranes and mitochondria from animal tissues and cells. Nat Protoc. 2009; 4:1582–90. https://doi.org/10.1038/nprot.2009.151 PMID:19816421

11. Hackett RA, Steptoe A. Type 2 diabetes mellitus and psychological stress - a modifiable risk factor. Nat Rev Endocrinol. 2017; 13:547–60. https://doi.org/10.1038/nrendo.2017.64 PMID:28664919

12. Lupien SJ, Juster RP, Raymond C, Marin MF. The effects of chronic stress on the human brain: from neurotoxicity, to vulnerability, to opportunity. Front Neuroendocrinol. 2018; 49:91–105. https://doi.org/10.1016/j.yfrne.2018.02.001 PMID:29421159

13. Picard M, McEwen BS. Psychological stress and mitochondria: a conceptual framework. Psychosom Med. 2018; 80:126–40. https://doi.org/10.1097/PSY.0000000000000544 PMID:29389735

14. Butterfield DA, Hardas SS, Lange ML. Oxidatively modified glyceraldehyde-3-phosphate dehydrogenase (GAPDH) and Alzheimer's disease: many pathways to neurodegeneration. J Alzheimers Dis. 2010; 20:369–93. https://doi.org/10.3233/JAD-2010-1375 PMID:20164570

15. Hu J, Adler K, Farah CA, Hastings MH, Sossin WS, Schacher S. Cell-specific PKM isoforms contribute to the maintenance of different forms of persistent long-term synaptic plasticity. J Neurosci. 2017; 37:2746–63. https://doi.org/10.1523/JNEUROSCI.2805-16.2017 PMID:28179558

16. Sathe G, Na CH, Renuse S, Madugundu AK, Albert M, Moghekar A, Pandey A. Quantitative Proteomic Profiling of Cerebrospinal Fluid to Identify Candidate Biomarkers for Alzheimer's Disease. Proteomics Clin Appl. 2019; 13:e1800105. https://doi.org/10.1002/prca.201800105 PMID:30578620

17. Kant S, Stopa EG, Johanson CE, Baird A, Silverberg GD. Choroid plexus genes for CSF production and brain homeostasis are altered in Alzheimer's disease. Fluids Barriers CNS. 2018; 15:34. https://doi.org/10.1186/s12987-018-0120-7 PMID:30541599

18. Chandrasekaran K, Hatanpää K, Brady DR, Rapoport SI. Evidence for physiological down-regulation of brain oxidative phosphorylation in Alzheimer's disease. Exp Neurol. 1996; 142:80–88. https://doi.org/10.1006/exnr.1996.0180 PMID:8912900

19. Wang S, Tian M, Yang R, Jing Y, Chen W, Wang J, Zheng X, Wang F. 6-gingerol ameliorates behavioral changes and atherosclerotic lesions in ApoE$^{-/-}$ mice exposed to chronic mild stress. Cardiovasc Toxicol. 2018; 18:420–30. https://doi.org/10.1007/s12012-018-9452-4 PMID:29605868

20. Huang Y, Mahley RW. Apolipoprotein E: Structure and function in lipid metabolism, neurobiology, and Alzheimer's diseases. Neurobiology of Disease. 2014; 72:3–12. https://doi.org/10.1016/j.nbd.2014.08.025 PMID:25173806

21. Liu CC, Liu CC, Kanekiyo T, Xu H, Bu G. Apolipoprotein E and Alzheimer disease: risk, mechanisms and therapy. Nat Rev Neurol. 2013; 9:106–18. https://doi.org/10.1038/nrneurol.2012.263 PMID:23296339

22. Ellis JM, Wong GW, Wolfgang MJ. Acyl coenzyme a thioesterase 7 regulates neuronal fatty acid metabolism to prevent neurotoxicity. Mol Cell Biol. 2013; 33:1869–82. https://doi.org/10.1128/MCB.01548-12 PMID:23459938

23. Marrs WR, Blankman JL, Horne EA, Thomazeau A, Lin YH, Coy J, Bodor AL, Muccioli GG, Hu SS, Woodruff G, Fung S, Lafourcade M, Alexander JP, et al. The serine hydrolase ABHD6 controls the accumulation and efficacy of 2-AG at cannabinoid receptors. Nat Neurosci. 2010; 13:951–57. https://doi.org/10.1038/nn.2601 PMID:20657592

24. Awerman JL, Romero LM. Chronic psychological stress alters body weight and blood chemistry in European starlings (Sturnus vulgaris). Comp Biochem Physiol A Mol Integr Physiol. 2010; 156:136–42. https://doi.org/10.1016/j.cbpa.2010.01.010 PMID:20096363

25. Ciechanover A, Kwon YT. Protein Quality Control by Molecular Chaperones in Neurodegeneration. Front Neurosci. 2017; 11:185. https://doi.org/10.3389/fnins.2017.00185 PMID:28428740

26. Veleri S, Punnakkal P, Dunbar GL, Maiti P. Molecular insights into the roles of rab proteins in intracellular dynamics and neurodegenerative diseases. Neuromolecular Med. 2018; 20:18–36. https://doi.org/10.1007/s12017-018-8479-9 PMID:29423895

27. Kvarta MD, Bradbrook KE, Dantrassy HM, Bailey AM, Thompson SM. Corticosterone mediates the synaptic and behavioral effects of chronic stress at rat hippocampal temporoammonic synapses. J Neurophysiol. 2015; 114:1713–24. https://doi.org/10.1152/jn.00359.2015 PMID:26180121

28. Samuels IS, Karlo JC, Faruzzi AN, Pickering K, Herrup K, Sweatt JD, Saitta SC, Landreth GE. Deletion of ERK2 mitogen-activated protein kinase identifies its key roles in cortical neurogenesis and cognitive function. J Neurosci. 2008; 28:6983–95. https://doi.org/10.1523/JNEUROSCI.0679-08.2008 PMID:18596172

29. Pei JJ, Braak H, An WL, Winblad B, Cowburn RF, Iqbal K, Grundke-Iqbal I. Up-regulation of mitogen-activated protein kinases ERK1/2 and MEK1/2 is associated with the progression of neurofibrillary degeneration in Alzheimer's disease. Brain Res Mol Brain Res. 2002; 109:45–55.

https://doi.org/10.1016/s0169-328x(02)00488-6 PMID:12531514

30. Vanguilder HD, Bixler GV, Sonntag WE, Freeman WM. Hippocampal expression of myelin-associated inhibitors is induced with age-related cognitive decline and correlates with deficits of spatial learning and memory. J Neurochem. 2012; 121:77–98. https://doi.org/10.1111/j.1471-4159.2012.07671.x PMID:22269040

31. Ruano D, Abecasis GR, Glaser B, Lips ES, Cornelisse LN, de Jong AP, Evans DM, Davey Smith G, Timpson NJ, Smit AB, Heutink P, Verhage M, Posthuma D. Functional gene group analysis reveals a role of synaptic heterotrimeric G proteins in cognitive ability. Am J Hum Genet. 2010; 86:113–25. https://doi.org/10.1016/j.ajhg.2009.12.006 PMID:20060087

32. Cottrell JR, Levenson JM, Kim SH, Gibson HE, Richardson KA, Sivula M, Li B, Ashford CJ, Heindl KA, Babcock RJ, Rose DM, Hempel CM, Wiig KA, et al. Working memory impairment in calcineurin knock-out mice is associated with alterations in synaptic vesicle cycling and disruption of high-frequency synaptic and network activity in prefrontal cortex. J Neurosci. 2013; 33:10938–49. https://doi.org/10.1523/JNEUROSCI.5362-12.2013 PMID:23825400

33. Peterson D, Munger C, Crowley J, Corcoran C, Cruchaga C, Goate AM, Norton MC, Green RC, Munger RG, Breitner JC, Welsh-Bohmer KA, Lyketsos C, Tschanz J, Kauwe JS, and Alzheimer's Disease Neuroimaging Initiative. Variants in PPP3R1 and MAPT are associated with more rapid functional decline in Alzheimer's disease: the Cache county dementia progression study. Alzheimers Dement. 2014; 10:366–71. https://doi.org/10.1016/j.jalz.2013.02.010 PMID:23727081

34. Laumonnier F, Cuthbert PC, Grant SG. The Role of Neuronal Complexes in Human X-Linked Brain Diseases. Am J Hum Genet. 2007; 80:205–20. https://doi.org/10.1086/511441 PMID:17236127

35. Satoh K, Takeuchi M, Oda Y, Deguchi-Tawarada M, Sakamoto Y, Matsubara K, Nagasu T, Takai Y. Identification of activity-regulated proteins in the postsynaptic density fraction. Genes Cells. 2002; 7:187–97. https://doi.org/10.1046/j.1356-9597.2001.00505.x PMID:11895482

36. Bonito-Oliva A, Barbash S, Sakmar TP, Graham WV. Nucleobindin 1 binds to multiple types of pre-fibrillar amyloid and inhibits fibrillization. Sci Rep. 2017; 7:42880. https://doi.org/10.1038/srep42880 PMID:28220836

37. Letronne F, Laumet G, Ayral AM, Chapuis J, Demiautte F, Laga M, Vandenberghe ME, Malmanche N, Leroux F, Eysert F, Sottejeau Y, Chami L, Flaig A, et al. ADAM30 downregulates APP-linked defects through cathepsin D activation in Alzheimer's disease. EBioMedicine. 2016; 9:278–92. https://doi.org/10.1016/j.ebiom.2016.06.002 PMID:27333034

38. Riemenschneider M, Blennow K, Wagenpfeil S, Andreasen N, Prince JA, Laws SM, Förstl H, Kurz A. The cathepsin D rs17571 polymorphism: effects on CSF tau concentrations in Alzheimer disease. Hum Mutat. 2006; 27:532–37. https://doi.org/10.1002/humu.20326 PMID:16652347

39. Tian L, Zhang K, Tian ZY, Wang T, Shang DS, Li B, Liu DX, Fang WG, Wang ZY, Chen YH. Decreased expression of cathepsin D in monocytes is related to the defective degradation of amyloid-β in Alzheimer's disease. J Alzheimers Dis. 2014; 42:511–20. https://doi.org/10.3233/JAD-132192 PMID:24898658

40. Liang LN, Zhan LB, Hu SY, Sui H, Chen J. Study on Regulation of Autophagy and Endoplasmic Reticulum Stress in Hypothalamus by Zi-Bu Pi-Yin Recipe among Spleen-yin Deficiency Diabetes-associated Cognitive Decline in Rats. World Sci Technol/Mod Tradit Chin Med. 2015; 17:1189–93. https://doi.org/10.11842/wst.2015.06.012

41. Janson J, Laedtke T, Parisi JE, O'Brien P, Petersen RC, Butler PC. Increased Risk of Type 2 Diabetes in Alzheimer Disease. Diabetes. 2004; 53:474–81. https://doi.org/10.2337/diabetes.53.2.474 PMID:14747300

42. Malone JI, Hanna S, Saporta S, Mervis RF, Park CR, Chong L, Diamond DM. Hyperglycemia not hypoglycemia alters neuronal dendrites and impairs spatial memory. Pediatr Diabetes. 2008; 9:531–39. https://doi.org/10.1111/j.1399-5448.2008.00431.x PMID:19067891

43. Atamna H, Frey WH 2nd. Mechanisms of mitochondrial dysfunction and energy deficiency in Alzheimer's disease. Mitochondrion. 2007; 7:297–310. https://doi.org/10.1016/j.mito.2007.06.001 PMID:17625988

44. Walls KC, Coskun P, Gallegos-Perez JL, Zadourian N, Freude K, Rasool S, Blurton-Jones M, Green KN, LaFerla FM. Swedish Alzheimer mutation induces mitochondrial dysfunction mediated by HSP60 mislocalization of amyloid precursor protein (APP) and beta-amyloid. J Biol Chem. 2012; 287:30317–27. https://doi.org/10.1074/jbc.M112.365890 PMID:22753410

45. Shi X, Lu XG, Zhan LB, Qi X, Liang LN, Hu SY, Yan Y, Zhao SY, Sui H, Zhang FL. The effects of the Chinese medicine ZiBu PiYin recipe on the hippocampus in a rat model of diabetes-associated cognitive decline: a proteomic analysis. Diabetologia. 2011; 54:1888–99. https://doi.org/10.1007/s00125-011-2147-z PMID:21509442

46. Ma JH, Shen S, Wang JJ, He Z, Poon A, Li J, Qu J, Zhang SX. Comparative proteomic analysis of the mitochondria-associated ER membrane (MAM) in a long-term type 2 diabetic rodent model. Sci Rep. 2017; 7:2062. https://doi.org/10.1038/s41598-017-02213-1 PMID:28522876

47. Poston CN, Krishnan SC, Bazemore-Walker CR. In-depth proteomic analysis of mammalian mitochondria-associated membranes (MAM). J Proteomics. 2013; 79:219–30. https://doi.org/10.1016/j.jprot.2012.12.018 PMID:23313214

48. Sala-Vila A, Navarro-Lérida I, Sánchez-Alvarez M, Bosch M, Calvo C, López JA, Calvo E, Ferguson C, Giacomello M, Serafini A, Scorrano L, Enriquez JA, Balsinde J, et al. Interplay between hepatic mitochondria-associated membranes, lipid metabolism and caveolin-1 in mice. Sci Rep. 2016; 6:27351. https://doi.org/10.1038/srep27351 PMID:27272971

49. Adjei T, Xue J, Mandic DP. The Female Heart: Sex Differences in the Dynamics of ECG in Response to Stress. Front Physiol. 2018; 9:1616. https://doi.org/10.3389/fphys.2018.01616 PMID:30546313

50. Gu C, Zhou W, Wang W, Xiang H, Xu H, Liang L, Sui H, Zhan L, Lu X. ZiBuPiYin recipe improves cognitive decline by regulating gut microbiota in Zucker diabetic fatty rats. Oncotarget. 2017; 8:27693–703. https://doi.org/10.18632/oncotarget.14611 PMID:28099913

SUPPLEMENTARY MATERIALS

Quantitative proteomic analysis

Digestion of MAM samples and iTRAQ labeling

100 μl of each sample was digested in parallel via filter-aided sample preparation (FASP). The critical steps of the FASP method are: 200 μl UA buffer (8 M urea and 150 mM Tris-HCl pH 8.0) were added to each sample. DTT was added to the mixed sample to a final concentration of 100 mM and allowed to stand at room temperature for 1.5 h. Then the sample mixture was transferred to an ultrafiltration filter (30 kDa cutoff, Sartorius, Germany) and centrifuged at 13,000×*g* for 20 min, then washed again with UA buffer. Subsequently, 100 μl iodoacetamide solution (50 mM iodoacetamide in UA buffer) was added to the filter. The filter unit was mixed for 1 min followed by incubation for 30 min at room temperature in the dark and centrifuged at 13,000×*g* for 20 min. Two wash steps with 100 μl UA buffer were performed with centrifugation at 13,000×*g* for 20 min after each wash step. Then, 100 μl NH_4HCO_3 buffer (Sigma, St. Louis., MO) was added to the filter and centrifuged at 13,000×*g* for 15 min; this step was repeated thrice. Finally, 40 μl of trypsin (Promega, Madison, WI) buffer (3 μg trypsin in 40 μl NH_4HCO_3 buffer) was added and digested at 37° C for 16–18 h. The filter unit was transferred to a new tube and centrifuged at 13,000×*g* for 30 min. The resulting peptides were collected as a filtrate and desalted with a C18-SD Extraction Disk Cartridge (66872-U Sigma). The peptide concentration was analyzed by OD_{280}.

Subsequently, 50 μg of peptides per sample were labeled with iTRAQ reagents according to the manufacturer's instructions (iTRAQ Reagent-8plex Multiplex Kit, Applied Biosystems SCIEX, Foster City, CA). The MAM samples from ZDF were labeled with reagent 116, the MAM samples from PSD were labeled with reagent 114, the MAM samples from PDZ were labeled with reagent 115, and the IS were labeled with reagent 117. The labeling solution reaction was incubated at room temperature for 1 h prior to further analysis. Then, three independent biological experiments were performed for triplicate LC-MS/MS analyses.

EASY-nLC1000 separation

The column was equilibrated for 20 min with 95% (v/v) solvent A (0.1% (v/v) formic acid in Milli-Q water). Peptide mixtures were first flushed into a sample column, the Thermo Scientific EASY column (2 cm×100 μm, 5 μm-C18), then separated with an analytical column, the Thermo Scientific EASY column (75 μm×100 mm, 3 μm-C18), at 250 nl/min with solvent B (acetonitrile with 0.1% (v/v) formic acid, acetonitrile 84%) using a segmented gradient from 0-55% (v/v) for 220 min, from 55-100% (v/v) for 8 min, and then at 100% (v/v) for 12 min.

MS/MS analysis and quantification

The Q-Exactive (Thermo Finnigan, San Jose, CA) mass spectrometer was set to perform data acquisition in positive ion mode with a selected mass range of 350-1800 mass/charge (*m/z*). The resolving power for the Q-Exactive was set as 70,000 for the MS scan and 17,500 for the MS/MS scan at *m/z* 200. MS/MS data were acquired using the top 10 most abundant precursor ions with charge ≥2 as determined from the MS scan. These were selected with an isolation window of 2 *m/z* and fragmented by higher energy collisional dissociation with normalized collision energies of 29 eV. The maximum ion injection times for the survey scan and the MS/MS scans were 20 and 60 ms, respectively, and the automatic gain control target values for the MS scan mode was set to 3e6. Dynamic exclusion for selected precursor ions was set at 30 s. The underfill ratio was defined as 0.1% on the Q-Exactive.

Raw files were processed using Mascot 2.2 and Proteome Discoverer 1.4 (Thermo). The raw files were searched using the MASCOT engine (Matrix Science, London, UK; v2.2) embedded into Proteome Discoverer 1.4, against the Uniprot Rat database (02-28-2015, 34164 entries). The following search parameters were set: monoisotopic mass values, fragment mass tolerance at 0.1 Da and peptide mass tolerance ± 20 ppm, trypsin as the enzyme, and allowing up to 2 missed cleavages. Fixed modifications were defined as iTRAQ labeling and carbamidomethylation of cysteine; oxidation of methionine was specified as a variable modification. The decoy database pattern was set as the reversed version of the target database. All reported data were based on 99% confidence for peptide identification as determined by a false discovery rate (FDR) of no more than 1%. Protein identification was supported by at least one unique peptide identification.

The iTRAQ analysis of relative protein quantification levels across multiple samples was as follows. Proteome Discoverer 1.4 was used to calculate relative ratios of identified peptides among labeled samples using relative peak intensities of released iTRAQ reporter ions in each of the MS/MS spectra, while relative protein quantification among samples was based on weighted ratios of uniquely identified peptides that

belonged to the specific individual protein in which sample IS was used as a reference. Final ratios of protein quantification were then normalized by the median average protein quantification ratio for unequally mixed differently labeled samples. This correction is based on the assumption that the expression of most proteins does not change. Thus, if samples from each experimental condition are not combined in exactly equal amounts, this normalization fixes the systematic error. Only protein identification that was inferred from the unique peptide identification in all three independent experiments was considered.

Supplementary Tables

Supplementary Table 1. Identified proteins known to localize in MAM and associated with diabetes mellitus and cognitive impairment-related disease (UP: unique peptides).

Gene	Diabetes mellitus associated proteins	UP	Note
Nefl	Neurofilament light polypeptide	20	a
Hspd1	60 kDa heat shock protein, mitochondrial	17	a, b
Dld	Dihydrolipoyl dehydrogenase, mitochondrial	13	a, b
Mog	Myelin-oligodendrocyte glycoprotein	10	a
Syn2	Synapsin II, isoform CRA_a	10	a
Map6	Microtubule-associated protein 6	10	b
Gsn	Gelsolin	9	a
Sv2a	Synaptic vesicle glycoprotein 2A	9	a
Psap	Prosaposin	9	a
Ctsd	Cathepsin D	7	a, b
Lrp1	LDL receptor related protein 1	7	a
Marcks	Myristoylated alanine-rich C-kinase substrate	7	a
Nefh	Neurofilament heavy polypeptide	7	a
COX2	cytochrome c oxidase subunit II	6	a, b
Apoe	Apolipoprotein E	5	a, b, c
Pdk1	[Pyruvate dehydrogenase (acetyl-transferring)] kinase isozyme 1, mitochondrial	5	a
S100b	Protein S100-B	4	a, b, c
Eef1a2	Elongation factor 1-alpha 2	4	a, b
Pip4k2b	Phosphatidylinositol-5-phosphate 4-kinase type 2 beta	4	a
Mapk1	Mitogen-activated protein kinase 1	3	a, b
ALG2	ALG2, alpha-1,3/1,6-mannosyltransferase	3	a
Cdc42	Cell division control protein 42 homolog	3	a
Cisd2	CDGSH iron sulfur domain 2	3	a, b, c
Dctn1	Dynactin subunit 1	3	a
Fis1	Mitochondrial fission 1 protein	2	a, c
Tmed10	Transmembrane emp24 domain-containing protein 10	2	a
Dnajc5	DnaJ homolog subfamily C member 5	2	a
Vti1b	Vesicle transport through interaction with t-SNAREs homolog 1B	2	a
Gapdh	Glyceraldehyde-3-phosphate dehydrogenase	1	a, b
ND2	NADH-ubiquinone oxidoreductase chain 2	1	a
Lamp2	Lysosome-associated membrane glycoprotein 2	1	a
Psmd2	26S proteasome non-ATPase regulatory subunit 2	1	a
Cnnm1	Cyclin M1 (Predicted)	1	a
Dbnl	Drebrin-like protein	1	b
Bcap31	B-cell receptor-associated protein 31	1	c

a, Cognitive impairment-related disease associated proteins; b, Diabetes mellitus-associated proteins; c, Known MAM-localized proteins.

Supplementary Table 2. Functional clusters of significant MAM protein changes in PSD:ZDF group.

Sequence name	Gene name	Protein name	UP	FC	p-value
Q6AY58	Bcap31	B-cell receptor-associated protein 31	1	2.68	0.0203
F1LLX8	Lamp2	Lysosome-associated membrane glycoprotein 2	1	2.25	0.0498
Q6IFW6	Krt10	Keratin, type I cytoskeletal 10	6	2.18	0.0367
P30009	Marcks	Myristoylated alanine-rich C-kinase substrate	7	1.48	0.0027
Q68FQ0	Cct5	T-complex protein 1 subunit epsilon	9	1.44	0.0258
Q4FZT9	Psmd2	26S proteasome non-ATPase regulatory subunit 2	1	1.42	0.0130
Q7TNM3	OMG	Oligodendrocyte-myelin glycoprotein	7	1.42	0.0127
P13638	Atp1b2	Sodium/potassium-transporting ATPase subunit beta-2	5	1.39	0.0300
Q9Z270	Vapa	Vesicle-associated membrane protein-associated protein A	6	1.38	0.0276
Q6JAM9	Tmem35	Transmembrane protein 35	1	1.38	0.0094
D3ZEI4	Hepacam	Hepatocyte cell adhesion molecule	3	1.37	0.0308
P31647	Slc6a11	Sodium- and chloride-dependent GABA transporter 3	8	1.37	0.0464
P02650	Apoe	Apolipoprotein E	5	1.34	0.0421
B0BNM7	Sco1	Sco1 protein	1	1.34	0.0130
Q6AY84	Scrn1	Secernin-1	5	1.32	0.0062
O88377	Pip4k2b	Phosphatidylinositol 5-phosphate 4-kinase type-2 beta	4	1.32	0.0283
P23562	Slc4a1	Band 3 anion transport protein	8	1.32	0.0086
P63086	Mapk1	Mitogen-activated protein kinase 1	3	1.32	0.0192
Q63345	Mog	Myelin-oligodendrocyte glycoprotein	10	1.32	0.0342
Q812E9	Gpm6a	Neuronal membrane glycoprotein M6-a	5	1.29	0.0495
Q6PST4	Atl1	Atlastin-1	3	1.28	0.0175
D4AAE9	Cisd2	CDGSH iron sulfur domain 2	3	1.28	0.0167
G3V7P1	Stx12	Syntaxin-12	3	1.27	0.0016
Q3MHS9	Cct6a	Chaperonin containing Tcp1, subunit 6A (Zeta 1)	7	1.27	0.0099
Q5RKJ9	RAB10	RAB10, member RAS oncogene family	6	1.26	0.0105
F1LMR7	Dpp6	Dipeptidyl aminopeptidase-like protein 6	9	1.26	0.0169
Q68FP1	Gsn	Gelsolin	9	1.26	0.0487
G3V9B3	Mag	Myelin-associated glycoprotein	10	1.25	0.0017
Q02563	Sv2a	Synaptic vesicle glycoprotein 2A	9	1.24	0.0444
Q5RKI0	Wdr1	WD repeat-containing protein 1	8	1.24	0.0372
A0A096MJM1	Rhog	Ras homolog family member G	7	1.24	0.0019
P62909	Rps3	40S ribosomal protein S3	3	1.23	0.0125
P63322	Rala	Ras-related protein Ral-A	4	1.22	0.0347
Q6PEC4	Skp1	S-phase kinase-associated protein 1	3	1.22	0.0027
Q5FVQ4	Mlec	Malectin	3	1.22	0.0167
P97710	Sirpa	Tyrosine-protein phosphatase non-receptor type substrate 1	6	1.21	0.0176
B0BNM1	Apoa1bp	NAD(P)H-hydrate epimerase	3	0.83	0.0340
P63100	Ppp3r1	Calcineurin subunit B type 1	6	0.83	0.0433
G3V6P8	Gng12	Guanine nucleotide-binding protein subunit gamma	3	0.82	0.0103
P23965	Eci1	Enoyl-CoA delta isomerase 1, mitochondrial	7	0.82	0.0254
G3V733	Syn2	Synapsin II, isoform CRA_a	10	0.82	0.0197
Q5XIH3	Ndufv1	NADH dehydrogenase [ubiquinone] flavoprotein 1, mitochondrial	16	0.81	0.0425
P38718	Mpc2	Mitochondrial pyruvate carrier 2	3	0.81	0.0186
Q09073	Slc25a5	ADP/ATP translocase 2	2	0.81	0.0123
Q5EBA4	Nipsnap1	Nipsnap1 protein	7	0.79	0.0426
F1M6X5	Txnrd2	Thioredoxin reductase 2, mitochondrial	6	0.78	0.0449
P19627	Gnaz	Guanine nucleotide-binding protein G(z) subunit alpha	5	0.78	0.0298
P41565	Idh3g	Isocitrate dehydrogenase [NAD] subunit gamma 1, mitochondrial	8	0.78	0.0090
P60905	Dnajc5	DnaJ homolog subfamily C member 5	2	0.77	0.0353

D4A1C0	Cnnm1	Cyclin M1 (Predicted)	1	0.76	0.0407
B2GV06	Oxct1	Succinyl-CoA:3-ketoacid coenzyme A transferase 1, mitochondrial	17	0.76	0.0343
G3V6H5	Slc25a11	Mitochondrial 2-oxoglutarate/malate carrier protein	13	0.75	0.0444
Q80W89	Ndufa11	NADH dehydrogenase [ubiquinone] 1 alpha subcomplex subunit 11	3	0.74	0.0145
F1MA54	Pdk1	[Pyruvate dehydrogenase (acetyl-transferring)] kinase isozyme 1, mitochondrial	5	0.74	0.0411
F1LRZ7	Nefh	Neurofilament heavy polypeptide	7	0.72	0.0150
Q6TUG0	Dnajb11	DnaJ homolog subfamily B member 11	1	0.72	0.0287
F8WG67	Acot7	Acyl-CoA thioesterase 7, isoform CRA_a	3	0.71	0.0040
B4F7C2	Tubb4a	Tubulin beta chain	5	0.70	0.0201
B2GV73	Arpc3	Actin-related protein 2/3 complex subunit 3	1	0.69	0.0095
A0A097PE04	COX2	Cytochrome c oxidase subunit 2	6	0.69	0.0311
Q6P6R2	Dld	Dihydrolipoyl dehydrogenase, mitochondrial	13	0.68	0.0303
Q8CFN2	Cdc42	Cell division control protein 42 homolog	3	0.68	0.0243
P56522	Fdxr	NADPH:adrenodoxin oxidoreductase, mitochondrial	9	0.68	0.0084
Q9R170	Bcat1	Branched-chain-amino-acid aminotransferase	3	0.68	0.0341
P49432	Pdhb	Pyruvate dehydrogenase E1 component subunit beta, mitochondrial	13	0.66	0.0235
P63039	Hspd1	60 kDa heat shock protein, mitochondrial	17	0.65	0.0438
Q6PDU7	Atp5l	ATP synthase subunit g, mitochondrial	3	0.64	0.0007
P19527	Nefl	Neurofilament light polypeptide	20	0.64	0.0170
P04631	S100b	Protein S100-B	4	0.64	0.0053
B0BNK1	Rab5c	RAB5C, member RAS oncogene family	4	0.63	0.0087
Q5I0L3	Yars2	Tyrosine--tRNA ligase, mitochondrial	2	0.63	0.0157
Q9JHL4	Dbnl	Drebrin-like protein	1	0.59	0.0112
Q6P7S0	Pkm	Pyruvate kinase	2	0.58	0.0106
P28023	Dctn1	Dynactin subunit 1	3	0.58	0.0256
Q6AYT7	Abhd12	Monoacylglycerol lipase ABHD12	1	0.56	0.0410
Q63083	Nucb1	Nucleobindin-1	2	0.56	0.0479
Q5XIG4	Ociad1	OCIA domain-containing protein 1	1	0.54	0.0040
P84817	Fis1	Mitochondrial fission 1 protein	2	0.53	0.0175
D4A7V1	Sh3glb2	Endophilin-B2	4	0.50	0.0353
P04797	Gapdh	Glyceraldehyde-3-phosphate dehydrogenase	1	0.46	0.0095
Q06QE9	ND2	NADH-ubiquinone oxidoreductase chain 2	1	0.42	0.0158
F1LNC4	Vti1b	Vesicle transport through interaction with t-SNAREs homolog 1B	2	0.40	0.0218
Q6Q0N1	Cndp2	Cytosolic non-specific dipeptidase	3	0.33	0.0048
Q45QL2	Gnb4	Guanine nucleotide binding protein beta-4	2	0.33	0.0416
G3V6U3	Alg2	ALG2, alpha-1,3/1,6-mannosyltransferase	3	0.31	0.0033

The color gradient of green and yellow were used to visualize the increased or decreased abundances of PSD proteins compared to the ZDF group, respectively (FC: fold change).

Supplementary Table 3. Functional clusters of significant MAM protein changes in PDZ:PSD group.

Sequence name	Gene name	Protein name	UP	FC	p-value
G3V6U3	Alg2	ALG2, alpha-1,3/1,6-mannosyltransferase	3	2.87	0.0070
Q6Q0N1	Cndp2	Cytosolic non-specific dipeptidase	3	2.27	0.0088
Q6AYT7	Abhd12	Monoacylglycerol lipase ABHD12	1	2.07	0.0453
W0NT55	Slc4a10	Anion exchange protein	3	1.82	0.0214
P04631	S100b	Protein S100-B	4	1.73	0.0095
P84817	Fis1	Mitochondrial fission 1 protein	2	1.70	0.0418
P04797	Gapdh	Glyceraldehyde-3-phosphate dehydrogenase	1	1.67	0.0473
Q06QE9	ND2	NADH-ubiquinone oxidoreductase chain 2	1	1.66	0.0315
Q3T1K5	Capza2	F-actin-capping protein subunit alpha-2	2	1.63	0.0391
Q6P7S0	Pkm	Pyruvate kinase	2	1.51	0.0267
D3ZZ21	Ndufb6	NADH dehydrogenase (Ubiquinone) 1 beta subcomplex, 6 (Predicted)	1	1.47	0.0273
Q6P7A4	Psap	Prosaposin	9	1.45	0.0496
Q9JHL4	Dbnl	Drebrin-like protein	1	1.44	0.0461
Q6PDU7	Atp5l	ATP synthase subunit g, mitochondrial	3	1.42	0.0414
B0BNK1	Rab5c	RAB5C, member RAS oncogene family	4	1.41	0.0138
Q6TUG0	Dnajb11	DnaJ homolog subfamily B member 11	1	1.37	0.0423
P24268	Ctsd	Cathepsin D	7	1.36	0.0141
Q63584	Tmed10	Transmembrane emp24 domain-containing protein 10	2	1.36	0.0089
P56522	Fdxr	NADPH:adrenodoxin oxidoreductase, mitochondrial	9	1.33	0.0155
F1M6X5	Txnrd2	Thioredoxin reductase 2, mitochondrial	6	1.32	0.0462
Q9R170	Bcat1	Branched-chain-amino-acid aminotransferase, cytosolic	3	1.28	0.0449
F8WG67	Acot7	Acyl-CoA thioesterase 7, isoform CRA_a	3	1.28	0.0352
Q62703	Rcn2	Reticulocalbin-2	4	1.23	0.0254
G3V6P8	Gng12	Guanine nucleotide-binding protein subunit gamma	3	1.23	0.0009
G3V928	Lrp1	LDL receptor-related protein 1	7	1.21	0.0329
Q63560	Map6	Microtubule-associated protein 6	10	0.83	0.0393
P02650	Apoe	Apolipoprotein E	5	0.83	0.0359
G3V9B3	Mag	Myelin-associated glycoprotein	10	0.83	0.0041
P62632	Eef1a2	Elongation factor 1-alpha 2	4	0.81	0.0137
Q63327	Mobp	Myelin-associated oligodendrocyte basic protein	3	0.81	0.0261
P63086	Mapk1	Mitogen-activated protein kinase 1	3	0.80	0.0295
Q7TNM3	OMG	Oligodendrocyte-myelin glycoprotein	7	0.77	0.0290
O35987	Nsfl1c	NSFL1 cofactor p47	1	0.66	0.0028

The color gradient of green and yellow were used to visualize the increased or decreased abundances of PDZ proteins compared to the PSD group, respectively.

Supplementary Table 4. Functional clusters of significant MAM protein changes in PSD:ZDF and PDZ:PSD groups.

Sequence name	Gene name	Protein name	UP	PSD: ZDF		PDZ:PSD	
				FC	p-value	FC	p-value
Q7TNM3	OMG	Oligodendrocyte-myelin glycoprotein	7	1.42	0.0127	0.77	0.0290
P02650	Apoe	Apolipoprotein E	5	1.34	0.0421	0.83	0.0359
P63086	Mapk1	Mitogen-activated protein kinase 1	3	1.32	0.0192	0.80	0.0295
G3V9B3	Mag	Myelin-associated glycoprotein	10	1.25	0.0017	0.83	0.0041
G3V6P8	Gng12	Guanine nucleotide-binding protein subunit gamma	3	0.82	0.0103	1.23	0.0009
F1M6X5	Txnrd2	Thioredoxin reductase 2, mitochondrial	6	0.78	0.0449	1.32	0.0462
Q6TUG0	Dnajb11	DnaJ homolog subfamily B member 11	1	0.72	0.0287	1.37	0.0423
F8WG67	Acot7	Acyl-CoA thioesterase 7, isoform CRA_a	3	0.71	0.0040	1.28	0.0352
P56522	Fdxr	NADPH:adrenodoxin oxidoreductase, mitochondrial	9	0.68	0.0084	1.33	0.0155
Q9R170	Bcat1	Branched-chain-amino-acid aminotransferase, cytosolic	3	0.68	0.0341	1.28	0.0449
Q6PDU7	Atp5l	ATP synthase subunit g, mitochondrial	3	0.64	0.0007	1.42	0.0414
P04631	S100b	Protein S100-B	4	0.64	0.0053	1.73	0.0095
B0BNK1	Rab5c	RAB5C, member RAS oncogene family	4	0.63	0.0087	1.41	0.0138
D3ZQQ5	Dnm1	Dynamin-1	4	0.60	0.0133	1.50	0.0445
Q9JHL4	Dbnl	Drebrin-like protein	1	0.59	0.0112	1.44	0.0461
Q6P7S0	Pkm	Pyruvate kinase	2	0.58	0.0106	1.51	0.0267
Q6AYT7	Abhd12	Monoacylglycerol lipase ABHD12	1	0.56	0.0410	2.07	0.0453
P84817	Fis1	Mitochondrial fission 1 protein	2	0.53	0.0175	1.70	0.0418
P04797	Gapdh	Glyceraldehyde-3-phosphate dehydrogenase	1	0.46	0.0095	1.67	0.0473
Q06QE9	ND2	NADH-ubiquinone oxidoreductase chain 2	1	0.42	0.0158	1.66	0.0315
Q6Q0N1	Cndp2	Cytosolic non-specific dipeptidase	3	0.33	0.0048	2.27	0.0088
G3V6U3	Alg2	ALG2, alpha-1,3/1,6-mannosyltransferase	3	0.31	0.0033	2.87	0.0070

The color gradient of green and yellow were used to visualize the increased or decreased abundances, respectively.

Supplementary Table 5. Antibodies applied in Western blotting (WB).

Antibody	WB Dilution	Catalog No.	Provider
anti-FACL4	1:1000	ab155282	Abcam
anti-cytochrome c	1:500	4280	Cell Signaling Technology
anti-alpha tubulin	1: 1000	ab176560	Abcam
anti-KDEL	1:1000	ADI-SPA-827-D	Enzo Life Sciences
anti-IP3 receptor 1	1:1000	8568	Cell Signaling Technology
anti-VDAC	1:1000	4866	Cell Signaling Technology
anti-PKM	1:500	ab38237	Abcam
anti ERK2	1:1000	ab32081	Abcam
anti-apolipoprotein E	1:500	ab183597	Abcam
anti-GAPDH	1:1000	5174	Cell Signaling Technology
anti-ALG2	1:1000	ab183597	Abcam